

Linear instability of interfacial Hele-Shaw flows of viscoelastic fluids

Zhiying Hai^a, Prabir Daripa^{b,*}

^aDepartment of Mathematics, Texas A&M University, 155 Ireland St, College Station, 77840, TX, USA

^bDepartment of Mathematics, Texas A&M University, 155 Ireland St, College Station, 77840, TX, USA

ARTICLE INFO

Keywords:

Saffman-Taylor
Viscous fingering
Hele-Shaw flow
Upper convected Maxwell fluid
Elastic fracturing

ABSTRACT

We present a theoretical study on the role of elasticity in causing fingering or fracturing instability during the immiscible displacement process of a viscoelastic fluid by another viscoelastic fluid in a rectilinear Hele-Shaw cell. Upper convected Maxwell (UCM) models are used for both fluid layers and linear stability analysis is performed in the regime of moderate to large Deborah number. This is a generalization of [20] where the case of a Newtonian fluid displacing an UCM fluid is considered. The elastic effect of the displacing layer has a significant impact on the overall flow stability. The dispersion relation is implicitly given a quartic polynomial equation with its coefficients depending on a modified wavenumber \tilde{k} , viscosity contrast η^r/η^l (displaced/displacing fluid), relaxation time contrast λ^r/λ^l and a composite parameter β inversely related to the flow speed U (depth averaged). Viscous effect is still the dominant mechanism in determining long wave stability (unstable if $\eta^r/\eta^l > 1$). The elastic effect of the displacing layer always destabilizes short waves (unstable if wavelength is shorter than $\lambda^l U$). In addition, three types of singular behaviors are found all of which are associated with elastic effects: (i) velocity becomes singular at infinitely many isolated wavenumbers (precise values are inversely proportional $\lambda^l U$ or $\lambda^r U$); (ii) stress becomes singular if wavenumber exceeds certain value (can happen even for slow flow); and (iii) growth rate becomes singular at up to two wavenumbers if η^r/η^l , λ^r/λ^l and β fall within a certain range but this can always be avoided if flow is slow enough. The special cases of an UCM fluid displacing air or a viscous Newtonian fluid are also considered.

1. Introduction

During the immiscible displacement of a more viscous fluid by a less viscous one in a Hele-Shaw cell, the fluid-fluid interface becomes unstable and develops into finger-like patterns. This process is commonly referred to as viscous fingering or Saffman-Taylor instability [44], although it appears that Hill [21] was the first one to study this problem. Due to its relevance in science and technology, considerable amount of research efforts have been devoted since the fifties in an attempt to better understand this phenomenon. Currently, such displacement processes are well understood when involved fluids are Newtonian and stability results are harnessed to the extent possible in controlling undesirable fingering stability (see [43, 22, 7] for a review).

Experimental investigations on non-Newtonian Hele-Shaw flows started in the eighties and strikingly different fingering patterns were observed, such as dendritic [6, 30], fractal [35, 10, 25, 53, 50, 48, 30] and fractures [25, 53, 49, 30, 32, 46, 2]. It comes as no surprise that there is no complete understanding for such differences because the morphology of fingering patterns strongly depends on the physiochemical nature of the fluids in addition to the usual parameters such as geometry of the cell, flow speed, and interfacial tension, etc.. The fluids generally can exhibit multiple non-Newtonian properties, such as shear-rate dependent viscosity, elasticity, yield-stress, etc., which can synergize or compete against each other for the overall flow dynamics. Disentangling different effects is essential to gain fundamental understanding of the pattern formation process. This is an extremely challenging task and requires simultaneous experimental [5, 37, 26, 28, 27, 29, 34, 45, 32, 2, 14, 15, 1] and theoretical

efforts [51, 42, 41, 24, 23, 9, 3, 16, 31, 32, 17, 2, 47]. We have cited only some works here from a huge body of literature in this area and we refer the readers to the above papers and references cited therein for a more complete overview overview of the field.

It is generally believed that shear-thinning effect promotes fractal growth, characterized by a highly ramified tip-splitting process. On the other hand, a transition from fractal pattern to fracturing [25, 53, 30, 49, 32, 46] is observed if the material relaxation time or flow speed are sufficiently increased (i.e. increased Deborah number) where the fingers become crack-like with sharp tips. In addition, there are also secondary cracks perpendicularly branching off the sides of the main cracks whereas the branching for classical Saffman-Taylor fingers or fractal type happens at the finger-tips. Since similar pattern is found in an elastic solid under sufficiently large tensile stress, it is natural to expect that elasticity must play a role in causing the fractures. However, this has received much less attention from the scientific community compared to other non-Newtonian effects.

The first theoretical attempt on the role of elastic effect was made by Wilson [51] who considered air displacing an Oldroyd-B fluid or an Upper convected Maxwell (UCM) fluid and studied the linear stability in the regime of moderate to high Deborah number. Since the averaging procedure used in the Newtonian case yielding Darcy's law is no longer valid, Wilson started with the full set of equations from which a system of linearized perturbation equations was obtained in the thin gap limit. Using a normal mode ansatz for the perturbations, the equations were then solved numerically to obtain the dispersion relations. A sharp increase, although remains finite, in the growth rate as Deborah number increases is predicted which the author

*Corresponding author, Email address: daripa@tamu.edu

ascribed to a resonance phenomenon. Mora and Manna [32] later considered the same problem (air displacing UCM) using a semi-analytical approach. They predicted a large growth rate near certain wavenumber, which eventually becomes singular when a combination of dimensionless groups exceeds a critical value. They also performed experiments and observed fracturing, thus establishing the connection of the resonance phenomenon to something observable in experiments. About the same time, Daripa [11, 12] studied the same problem with an Oldroyd-B fluid but neglecting the time derivative in the constitutive relation. There appears to be no physical or mathematical justification for this simplification except to make the problem analytically tractable. This subsequently led to an explicit formula for the dispersion relation which also shows the existence of singular growth rate in spite of gross simplification of the underlying modeling equations. Recently, Hai and Daripa [20] tackled the same problem where a viscous Newtonian fluid displaces an UCM fluid. The solution technique is analytical and produces the dispersion relation in closed form and recovers results obtained in [44, 51, 32] as special cases. Additional singular behaviors absent in [51, 32] are also discovered.

In this paper, we provide further insights on the role of elasticity in causing fingering or fracturing instability and generalize the results obtained by Hai and Daripa [20] by replacing the displacing Newtonian fluid with another UCM fluid. The development procedure is similar to that of [20] but is written in a self-contained manner at the expense of some degree of overlap.

This paper is organized as follows. In §2, the setup is described and the governing equations are presented. In §3, the equations are non-dimensionalized and a set of reduced equations is obtained in the thin gap limit while keeping the Deborah number to be of constant order or larger so that elastic effect is apparent. In §4, the equations are perturbed and linearized about the basic flow of form $\mathbf{u}_0 = (U(y), 0, 0)$. The method of normal mode is applied to the linearized equations, which then leads to a boundary value problem (BVP). The BVP is then solved analytically where the solution involves weighted integral of Bessel functions. In §5, the solution of BVP is then inserted into the interface conditions to obtain the eigenvalue relation $\mathcal{F} = 0$, where \mathcal{F} is a quartic polynomial in the growth rate with coefficients depending on wavenumber, along with several dimensionless groups as parameters. The detailed analysis on the roots is given where stable and unstable wave bands are identified and the effects of involved parameters are discussed. Several types of singular behaviors strongly related to elastic effect are discovered. The special cases where UCM displaces air or a viscous Newtonian fluid are also considered. Significant results from a physical perspective for all these cases are documented in this section. Three Appendices contain important details which lead to these results. Conclusions are made in §6.

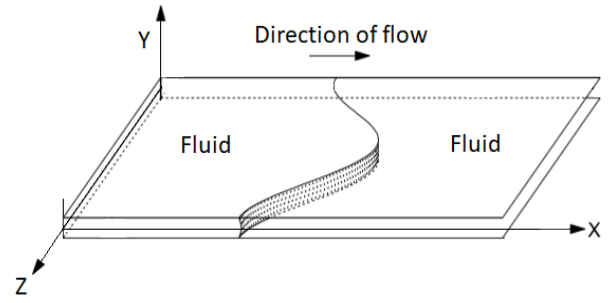


Figure 1: A section of the rectilinear Hele-Shaw flow

2. Setup Description and governing equations

Two fluids are confined in a rectilinear Hele-Shaw cell with a gap separation $2b$ and moving to the $+x$ direction due to a driving source located upstream ($-x$ direction). A section of the setup is shown in figure 1. The fluids are assumed to be immiscible, incompressible and homogeneous. The interface that separates the two fluids has constant interfacial tension γ . The wetting effect and y direction variation of the interface are neglected [36, 38, 41] and will be further discussed in the remark at the end of §3. We further assume that the interface can be described by an equation of form $x = \zeta(z, t)$. The displacing fluid occupies $x < \zeta(z, t)$ and the displaced fluid occupies $\zeta(z, t) < x$. Inertial terms and gravity effect are neglected.

The flow is governed by equations of continuity, momentum and UCM constitutive equation

$$\left. \begin{aligned} \nabla \cdot \mathbf{u} &= 0, & \nabla p &= \nabla \cdot \boldsymbol{\tau}, \\ \boldsymbol{\tau} + \lambda \frac{D_1 \boldsymbol{\tau}}{Dt} &= \eta (\nabla \mathbf{u} + (\nabla \mathbf{u})^T). \end{aligned} \right\} \quad (1)$$

where $\mathbf{u} = (u, v, w)$ is the velocity field with u, v, w as velocity components in the x, y, z directions respectively, p is the pressure, $\boldsymbol{\tau}$ is the extra stress tensor, λ and η are the material relaxation time and viscosity respectively. D_1/Dt is the upper convected time derivative.

All quantities involved in (1) are understood as piecewise functions with jump discontinuities across the interface $x = \zeta(z, t)$. Throughout the development, we use superscripts l and r to refer a quantity to be associated with the displacing and displaced layers respectively. We denote by $\langle \cdot \rangle$ the average across the gap direction, and by $[[\cdot]]$ the jump across the interface. Subscripts x, y and z denote the corresponding partial derivatives.

Non-slip and non-penetration conditions at the cell plates

$$\mathbf{u}|_{y=\pm b} = 0. \quad (2)$$

At the interface $x = \zeta(z, t)$, we impose gap averaged kinematic and dynamic conditions. The former states the interface velocity is the same as the average fluid velocity on the two sides

$$\zeta_t = \langle u^r \rangle - \langle w^r \rangle \zeta_z = \langle u^l \rangle - \langle w^l \rangle \zeta_z. \quad (3)$$

The latter states the discontinuity of the average normal stress is balanced by the curvature effect $-\langle\langle p \rangle\rangle + \mathbf{n} \cdot \langle\langle \boldsymbol{\tau} \rangle\rangle \mathbf{n} = \gamma \nabla \cdot \mathbf{n}$, where \mathbf{n} is the unit normal of the interface pointing into the displaced fluid. Equivalently, this reads

$$(1 + \zeta_z^2) \langle\langle p \rangle\rangle - \langle\langle \tau^{xx} \rangle\rangle - 2\langle\tau^{xz}\rangle\zeta_z + \langle\tau^{zz}\rangle\zeta_z^2 = \gamma \zeta_{zz} / (1 + \zeta_z^2)^{1/2}. \quad (4)$$

3. Lubrication approximation

Certain terms from (1)-(4) can be dropped in the thin gap limit owing to the Hele-Shaw geometry. To do so, a set of scales must be properly chosen first. Away from the interface, the dominant part of the flow field is parallel to the cell plates, therefore the relative sizes of physical variables can be captured by studying flow of the form $\mathbf{u} = (u(y), 0, 0)$ for which (1) reduces to

$$\left. \begin{aligned} p_x = \eta u_{yy}, \quad p_y = 0, \quad p_z = 0, \\ \tau^{xy} = \tau^{yx} = \eta u_y, \quad \tau^{xx} = 2\lambda u_y \tau^{xy}, \end{aligned} \right\} \quad (5)$$

where all other components of $\boldsymbol{\tau}$ are zero. From (5), we obtain the following scales

$$\left. \begin{aligned} x, z \propto L, \quad y \propto b, \quad u, w \propto V, \quad v \propto bV/L \\ t \propto L/V, \quad p \propto G, \quad \tau^{xy}, \tau^{yz} \propto \bar{\eta}V/b, \\ \tau^{xx}, \tau^{xz}, \tau^{zz} \propto \bar{\lambda}\bar{\eta}V^2/b^2, \quad \tau^{yy} \propto \bar{\eta}V/L, \end{aligned} \right\} \quad (6)$$

where L and V are the characteristic length and velocity scale in the lateral direction, b is the length scale in the transverse direction, G is a characteristic pressure, $\bar{\lambda} = \lambda^l + \lambda^r$, and $\bar{\eta} = \eta^l + \eta^r$. The use of $\bar{\eta}$ and $\bar{\lambda}$ is to have a consistent set of units for both fluid layers. The difference in viscosities and relaxation times of the two fluid layers are reflected in $R_\eta^{l,r}$ and $R_\lambda^{l,r}$ defined in (7) below, which will be carried into the scaled equations.

$$R_\lambda^{l,r} \stackrel{def}{=} \lambda^{l,r} / \bar{\lambda}, \quad R_\eta^{l,r} \stackrel{def}{=} \eta^{l,r} / \bar{\eta} \quad (7)$$

The following relation is obtained by balancing the units on the momentum equation

$$V = \epsilon^2 GL / \bar{\eta}. \quad (8)$$

Using the scaling scheme introduced above, non-dimensionalized showing the interface between layered fluids in a channel or pipe can become unstable, one may speculate that such instability in the thin film region could affect the leading interface. However, we believe the initial onset of instability of the leading interface will not be caused by that of the thin film region. But to fully address such an issue with rigor, perhaps a multi-scale analysis is necessary. This is because such investigations need to be done over a length scale on the order of b whereas the Hele-Shaw approximation assumes the separation of length scale $\epsilon = b/L \ll 1$, where

$$\epsilon \stackrel{def}{=} b/L, \quad De \stackrel{def}{=} \epsilon^2 G \bar{\lambda} / \bar{\eta}, \quad Ca \stackrel{def}{=} GL / \gamma, \quad (9)$$

where ϵ is the characteristic aspect ratio of the Hele-Shaw cell, De is the Deborah number, and Ca is the capillary number. In the thin gap limit $\epsilon \rightarrow 0$, elastic behavior is apparent if $De \sim O(1)$ or larger. Since the characteristic

pressure G is ultimately determined by the external driving source, G can be taken as an adjustable parameter to achieve this. For example, $De \sim O(1)$ if $G \sim O(\epsilon^{-2})$ by (9). In such a regime, the leading order equations obtained from (1)-(4) are given by (with slight risk of confusion, we have used the same symbols to denote the dimensionless quantities)

$$\left. \begin{aligned} u_x + v_y + w_z &= 0, & p_y &= 0, \\ p_x &= R_\eta (R_\lambda De (\tau_x^{xx} + \tau_z^{xz}) + \tau_y^{xy}), \\ p_z &= R_\eta (R_\lambda De (\tau_x^{xz} + \tau_z^{zz}) + \tau_y^{yz}), \\ L\tau^{xy} &= u_y + R_\lambda^2 De^2 (v_x \tau^{xx} + v_z \tau^{xz}) \dots \\ &+ R_\lambda De ((u_x + v_y) \tau^{xy} + u_z \tau^{yz} + u_y \tau^{yy}), \\ L\tau^{yz} &= w_y + R_\lambda^2 De^2 (v_x \tau^{xz} + v_z \tau^{zz}) \dots \\ &+ R_\lambda De ((w_z + v_y) \tau^{yz} + w_x \tau^{xy} + w_y \tau^{yy}), \\ L\tau^{xx} &= 2(u_y \tau^{xy} + R_\lambda De (u_x \tau^{xx} + u_z \tau^{xz})), \\ L\tau^{xz} &= u_y \tau^{yz} + w_y \tau^{xy} \dots \\ &+ R_\lambda De ((u_x + w_z) \tau^{xz} + u_z \tau^{zz} + w_x \tau^{xx}), \\ L\tau^{yy} &= 2(v_y + R_\lambda De (v_x \tau^{xy} + v_y \tau^{yy} + v_z \tau^{yz})), \\ L\tau^{zz} &= 2(w_y \tau^{yz} + R_\lambda De (w_z \tau^{zz} + w_x \tau^{xz})), \end{aligned} \right\} \quad (10)$$

where

$$L \stackrel{def}{=} I + R_\lambda De (\partial_t + u \partial_x + v \partial_y + w \partial_z). \quad (11)$$

At the cell plates $y = \pm 1$, $u = v = w = 0$. At the interface $x = \zeta(z, t)$,

$$\left. \begin{aligned} \zeta_t &= \langle u^l \rangle - \langle w^r \rangle \zeta_z, \\ \langle u^r \rangle - \langle w^r \rangle \zeta_z &= \langle u^l \rangle - \langle w^l \rangle \zeta_z, \\ \langle\langle (1 + \zeta_z^2) p - R_\eta R_\lambda De (\tau^{xx} - 2\tau^{xz} \zeta_z + \tau^{zz} \zeta_z^2) \rangle\rangle & \\ &= Ca^{-1} \zeta_{zz} / (1 + \zeta_z^2)^{1/2}. \end{aligned} \right\} \quad (12)$$

Remark: If the displaced fluid wets the walls, there will be a thin film left behind the interface. Over such a region, the flow essentially becomes a channel flow in $x-z$ plane where the two fluids are separated by an interface parallel to the channel walls. Since there are many works [52, 40, 8, 18, 19] showing the interface between layered fluids in a channel or pipe can become unstable, one may speculate that such instability in the thin film region could affect the leading interface. However, we believe the initial onset of instability of the leading interface will not be caused by that of the thin film region. But to fully address such an issue with rigor, perhaps a multi-scale analysis is necessary. This is because such investigations need to be done over a length scale on the order of b whereas the Hele-Shaw approximation assumes the separation of length scale $\epsilon = b/L \ll 1$, where

the primary length scale of interest L is in the spanwise direction (z). In other words, linear theory based on such approximation cannot capture any details over the length scale of order b or less. This is also the reason why we confined our later analysis to relatively long wavelength to preserve the reliability of the theory.

4. Linear stability

Now we consider the linear stability of the basic flow $\mathbf{u}_0 = (U(y), 0, 0)$ for equations (10) through (12). The basic solution satisfying $U(\pm 1) = 0$ is easily found to be

$$\left. \begin{aligned} U &= -3\langle U \rangle (y^2 - 1)/2, & \langle U \rangle &= -p_{0,x}/(3R_\eta), \\ \tau_0^{xy} &= U_y, & \tau_0^{xx} &= 2U_y \tau_0^{xy}, \end{aligned} \right\} \quad (13)$$

where $p_{0,x}$ is a negative constant. Interface conditions (12) give

$$\zeta_0 = \langle U \rangle t, \quad \llbracket \langle U \rangle \rrbracket = 0, \quad \llbracket p_0 - R_\eta R_\lambda De \langle \tau_0^{xx} \rangle \rrbracket = 0. \quad (14)$$

By (13)₂ and (14)₂

$$\llbracket p_{0,x} \rrbracket = -3\langle U \rangle \llbracket R_\eta \rrbracket. \quad (15)$$

Now we perturb equations (10) through (12) about the basic solution given by (13) and (14), and then linearize. This process is lengthy but straightforward thus omitted. On the resulting equations, a moving frame of reference $x \mapsto x - \langle U \rangle t$ is used, and the following normal mode ansatz is used for the perturbations (a two dimensional perturbation for the velocity field is assumed, namely $v_1 \equiv 0$).

$$(u_1, w_1, p_1, \tau_1^{ij}, \zeta_1) = (\hat{u}, \hat{w}, \hat{p}, \hat{\tau}^{ij}, \hat{\zeta}) e^{\mu t + ikz}, \quad (16)$$

where the quantities with hat are complex valued amplitudes, $\mu \in \mathbb{C}$ is the temporal growth rate of perturbations (real part understood) and k is the wavenumber in the z -direction (perpendicular to the direction of basic flow). The resulting equations for (10) are given by (17) below (obtained with $\hat{\tau}^{yy} = \hat{\tau}^{zz} = 0$ already have been applied. This is because they satisfy $L\hat{\tau}^{yy} = L\hat{\tau}^{zz} = 0$ where L is defined in (18)₁ below. The solutions for both are proportional to $\exp(-(1 + \mu De R_\lambda)x / (R_\lambda De V^*))$ with V^* given by (18)₂. Since V^* changes sign at $y = \pm 1/\sqrt{3}$, it must be $\hat{\tau}^{yy} = \hat{\tau}^{zz} = 0$ to be continuous).

$$\left. \begin{aligned} \hat{u}_x + ik\hat{w} &= 0, & \hat{p}_y &= 0, \\ \hat{p}_x &= R_\eta (R_\lambda De (\hat{\tau}_x^{xx} + ik\hat{\tau}_x^{xz}) + \hat{\tau}_y^{xy}), \\ ik\hat{p} &= R_\eta (R_\lambda De (\hat{\tau}_x^{xz} + \hat{\tau}_y^{yz}), \\ L\hat{\tau}^{xy} &= \hat{u}_y + R_\lambda De V_y^* \hat{u}_x, & L\hat{\tau}^{yz} &= \hat{w}_y + R_\lambda De V_y^* \hat{w}_x, \\ L\hat{\tau}^{xx} &= 2V_y^* (\hat{\tau}^{xy} + \hat{u}_y + 2R_\lambda De V_y^* \hat{u}_x), \\ L\hat{\tau}^{xz} &= V_y^* (\hat{\tau}^{yz} + \hat{w}_y + 2R_\lambda De V_y^* \hat{w}_x), \end{aligned} \right\} \quad (17)$$

where (the letter L is reused and not to be confused with (11))

$$\left. \begin{aligned} L &\stackrel{def}{=} (1 + \mu De R_\lambda)I + R_\lambda De V^* \partial_x, \\ V^* &\stackrel{def}{=} -3\langle U \rangle (y^2 - 1/3)/2. \end{aligned} \right\} \quad (18)$$

The corresponding interface condition (12) at $x = 0$ reads

$$\left. \begin{aligned} \mu \hat{\zeta} &= \langle \hat{u} \rangle, & \llbracket \langle \hat{u} \rangle \rrbracket &= 0, \\ \llbracket \hat{p} - R_\eta R_\lambda De \langle \hat{\tau}^{xx} \rangle \rrbracket &= (-k^2/Ca + 3\langle U \rangle \llbracket R_\eta \rrbracket) \hat{\zeta}, \end{aligned} \right\} \quad (19)$$

where (15) is used to obtain the second term on the right hand side of equation (19)₃.

From (17)₁, we obtain $L[\hat{\tau}_x^{xy} + ik\hat{\tau}_x^{yz}] = 0$ and $L[\hat{\tau}_x^{xx} + 2ik\hat{\tau}_x^{xz}] = 2V_y^* (\hat{\tau}_x^{xy} + ik\hat{\tau}_x^{yz})$. For the solutions to be continuous, it must be

$$\hat{\tau}_x^{xy} + ik\hat{\tau}_x^{yz} = 0, \quad \hat{\tau}_x^{xx} + 2ik\hat{\tau}_x^{xz} = 0. \quad (20)$$

By (20), (17)₃ and (17)₄, we obtain $\hat{p}_{xx} - k^2\hat{p} = 0$ which is satisfied by \hat{p}^l for $x < 0$ and \hat{p}^r for $x > 0$. The solution subject to the far field conditions $\hat{p}^l \rightarrow 0$ as $x \rightarrow -\infty$ and $\hat{p}^r \rightarrow 0$ as $x \rightarrow \infty$ is given by

$$\hat{p}^l = \hat{p}^- e^{|k|x}, \quad \hat{p}^r = \hat{p}^+ e^{-|k|x}, \quad (21)$$

for some constants \hat{p}^- and \hat{p}^+ . Applying the operator L to (17)₃

$$\begin{aligned} L\hat{p}_x/R_\eta &= R_\lambda De L[\hat{\tau}_x^{xx} + ik\hat{\tau}_x^{xz}] + L\hat{\tau}_y^{xy} \\ &= -R_\lambda De (ikL[\hat{\tau}_x^{xz}] + V_y^* \hat{\tau}_x^{xy}) + [L\hat{\tau}^{xy}]_y \\ &= -R_\lambda De (ikV_y^* (\hat{w}_y + 2R_\lambda De V_y^* \hat{w}_x) + V_y^* (\hat{\tau}_x^{xy} + \hat{\tau}_y^{yz})) \\ &\quad \dots + [\hat{u}_y + R_\lambda De V_y^* \hat{u}_x]_y \\ &= R_\lambda De V_y^* [\hat{u}_y + 2R_\lambda De V_y^* \hat{u}_x]_x + [\hat{u}_y + R_\lambda De V_y^* \hat{u}_x]_y. \end{aligned} \quad (22)$$

In the second equality above, (20)₂ is used along with the definition of L . (17)₅ and (17)₈ are used to obtain the third equality, and (17)₁, (20)₁ for the fourth. Substituting L and V^* given by (18) into (22), we obtain an equation of the form $E(\hat{u}, \hat{p}; R_\lambda, R_\eta, \mu, De, \langle U \rangle) = 0$ where E is a second order partial differential operator. The associated equation for the displacing (l) and the displaced (r) layers are respectively given by $E(\hat{u}^l, \hat{p}^l; R_\lambda^l, R_\eta^l, \mu, De, \langle U \rangle) = 0$ and $E(\hat{u}^r, \hat{p}^r; R_\lambda^r, R_\eta^r, \mu, De, \langle U \rangle) = 0$ where \hat{p}^l and \hat{p}^r are given by (21). These two equations are to be solved for \hat{u}^l and \hat{u}^r subject to $\hat{u}^l = \hat{u}^r = 0$ at $y = \pm 1$ with the far field conditions $\hat{u}^l \rightarrow 0$ as $x \rightarrow -\infty$ and $\hat{u}^r \rightarrow 0$ as $x \rightarrow \infty$. Using similar techniques introduced in Hai & Daripa [20, §5], the

solutions are given by

$$\left. \begin{aligned} \hat{u}^l &= (|k|\hat{\rho}^-/R_\eta^l)e^{|k|x}\hat{u}^l(y), \\ \hat{u}^l &\stackrel{def}{=} e^{R_\lambda^l\hat{k}y^2}(u_p^l - u_p^l(1)u_e^l/u_e^l(1)), \\ u_p^l &\stackrel{def}{=} u_o^l \int_0^y \psi^l u_e^l e^{-R_\lambda^l\hat{k}s^2} ds - u_e^l \int_0^y \psi^l u_o^l e^{-R_\lambda^l\hat{k}s^2} ds, \\ \psi^l &\stackrel{def}{=} \mu De R_\lambda^l + 1 + R_\lambda^l\hat{k}/3 - R_\lambda^l\hat{k}y^2, \\ u_e^l &\stackrel{def}{=} \Gamma(3/4)\hat{J}_{-1/4}(R_\lambda^l\hat{k}y^2), \\ u_o^l &\stackrel{def}{=} \Gamma(5/4)y\hat{J}_{1/4}(R_\lambda^l\hat{k}y^2). \end{aligned} \right\} \quad (23)$$

$$\left. \begin{aligned} \hat{u}^r &= -(|k|\hat{\rho}^+/R_\eta^r)e^{-|k|x}\hat{u}^r(y), \\ \hat{u}^r &\stackrel{def}{=} e^{-R_\lambda^r\hat{k}y^2}(u_p^r - u_p^r(1)u_e^r/u_e^r(1)), \\ u_p^r &\stackrel{def}{=} u_o^r \int_0^y \psi^r u_e^r e^{R_\lambda^r\hat{k}s^2} ds - u_e^r \int_0^y \psi^r u_o^r e^{R_\lambda^r\hat{k}s^2} ds, \\ \psi^r &\stackrel{def}{=} \mu De R_\lambda^r + 1 - R_\lambda^r\hat{k}/3 + R_\lambda^r\hat{k}y^2, \\ u_e^r &\stackrel{def}{=} \Gamma(3/4)\hat{J}_{-1/4}(R_\lambda^r\hat{k}y^2), \\ u_o^r &\stackrel{def}{=} \Gamma(5/4)y\hat{J}_{1/4}(R_\lambda^r\hat{k}y^2). \end{aligned} \right\} \quad (24)$$

where $\hat{J}_{\pm 1/4}$ is the analytic part of $J_{\pm 1/4}$, the Bessel function of first kind of order $\pm 1/4$, the Gamma values $\Gamma(3/4)$ and $\Gamma(5/4)$ are merely for convenience, and \hat{k} is a modified wavenumber given by

$$\hat{k} \stackrel{def}{=} 3|k|De\langle U \rangle/2. \quad (25)$$

5. Dispersion Relation

Substituting (23)₁ and (24)₁ into the right hand side of (17)₅, the stress $\hat{\tau}^{xy,l}$ and $\hat{\tau}^{xy,r}$ can be solved with integration

$$\left. \begin{aligned} R_\eta^l \hat{\tau}^{xy,l} &= |k|\hat{\rho}^- e^{|k|x} \hat{\tau}^{xy,l}, \\ \hat{\tau}^{xy,l} &\stackrel{def}{=} (\hat{u}_y^l + \psi_y^l \hat{u}^l)/\psi^l, \\ R_\eta^r \hat{\tau}^{xy,r} &= -|k|\hat{\rho}^+ e^{-|k|x} \hat{\tau}^{xy,r}, \\ \hat{\tau}^{xy,r} &\stackrel{def}{=} (\hat{u}_y^r + \psi_y^r \hat{u}^r)/\psi^r, \end{aligned} \right\} \quad (26)$$

Similarly, we obtain from (17)₇

$$\left. \begin{aligned} R_\eta^l R_\lambda^l De \hat{\tau}^{xx,l} &= 2\hat{\rho}^- e^{|k|x} \hat{\tau}^{xx,l}, \\ \hat{\tau}^{xx,l} &\stackrel{def}{=} (\hat{\tau}^{xy,l} + \hat{u}_y^l + 2\psi_y^l \hat{u}^l)\psi_y^l/\psi^l, \\ R_\eta^r R_\lambda^r De \hat{\tau}^{xx,r} &= 2\hat{\rho}^+ e^{-|k|x} \hat{\tau}^{xx,r}, \\ \hat{\tau}^{xx,r} &\stackrel{def}{=} (\hat{\tau}^{xy,r} + \hat{u}_y^r + 2\psi_y^r \hat{u}^r)\psi_y^r/\psi^r. \end{aligned} \right\} \quad (27)$$

The following relations are obtained by substituting (21), (20)₂ and (26) into (17)₃.

$$\begin{aligned} R_\eta^l R_\lambda^l De \hat{\tau}_x^{xx,l} &= 2\hat{\rho}^- |k|e^{|k|x}(1 - \hat{\tau}_y^{xy,l}), \\ R_\eta^r R_\lambda^r De \hat{\tau}_x^{xx,r} &= -2\hat{\rho}^+ |k|e^{-|k|x}(1 - \hat{\tau}_y^{xy,r}). \end{aligned}$$

By (27), it must be $\hat{\tau}^{xx,l} = 1 - \hat{\tau}_y^{xy,l}$ and $\hat{\tau}^{xx,r} = 1 - \hat{\tau}_y^{xy,r}$. As a result, taking the gap average gives (notice $\hat{\tau}^{xy,l}$ and $\hat{\tau}^{xy,r}$ are odd functions in y)

$$\begin{aligned} R_\eta^l R_\lambda^l De \langle \hat{\tau}^{xx,l} \rangle &= 2\hat{\rho}^- e^{|k|x}(1 - \hat{\tau}_y^{xy,l}(1)), \\ R_\eta^r R_\lambda^r De \langle \hat{\tau}^{xx,r} \rangle &= 2\hat{\rho}^+ e^{-|k|x}(1 - \hat{\tau}_y^{xy,r}(1)), \end{aligned}$$

or equivalently after using (26) and $\hat{u}^l(1) = \hat{u}^r(1) = 0$,

$$\left. \begin{aligned} R_\eta^l R_\lambda^l De \langle \hat{\tau}^{xx,l} \rangle &= 2\hat{\rho}^- e^{|k|x}(1 - \hat{u}_y^l(1)/\psi^l(1)), \\ R_\eta^r R_\lambda^r De \langle \hat{\tau}^{xx,r} \rangle &= 2\hat{\rho}^+ e^{-|k|x}(1 - \hat{u}_y^r(1)/\psi^r(1)). \end{aligned} \right\} \quad (28)$$

Using (19)₁, (19)₂, (23)₁, (24)₁ and (28), the dynamic condition (19)₃ becomes

$$\begin{aligned} \mu R_\eta^l \frac{2\hat{u}_y^l(1)/\psi^l(1) - 1}{\langle \hat{u}^l \rangle} + \mu R_\eta^r \frac{2\hat{u}_y^r(1)/\psi^r(1) - 1}{\langle \hat{u}^r \rangle} \\ = |k|^3 Ca^{-1} - 3\langle U \rangle |k| \llbracket R_\eta \rrbracket. \end{aligned} \quad (29)$$

From the definitions given in (23) and (24), it is clear that \hat{u}^l and \hat{u}^r can be written as

$$\left. \begin{aligned} \hat{u}^l &= \mu De R_\lambda^l \hat{u}_1^l(y; R_\lambda^l \hat{k}) + \hat{u}_2^l(y; R_\lambda^l \hat{k}), \\ \hat{u}^r &= \mu De R_\lambda^r \hat{u}_1^r(y; R_\lambda^r \hat{k}) + \hat{u}_2^r(y; R_\lambda^r \hat{k}). \end{aligned} \right\} \quad (30)$$

Eliminating $|k|$ in favor of \hat{k} by (25) from the right hand side of (29) and substituting (30) into the left hand side along with ψ^l and ψ^r given by (23)₄ and (24)₄ respectively gives

$$\begin{aligned} \frac{R_\eta^l \hat{\mu} z^l (\hat{\mu} R_\lambda^l + y^l)}{(\hat{\mu} R_\lambda^l + M^l \hat{k})(\hat{\mu} R_\lambda^l + x^l)} + \frac{R_\eta^r \hat{\mu} z^r (\hat{\mu} R_\lambda^r + y^r)}{(\hat{\mu} R_\lambda^r + M^r)(\hat{\mu} R_\lambda^r + x^r)} \\ = \beta \hat{k}^3 - 2\hat{k} \llbracket R_\eta \rrbracket, \end{aligned} \quad (31)$$

where

$$\left. \begin{aligned} \hat{\mu} &\stackrel{def}{=} \mu De, \quad \beta \stackrel{def}{=} 1/(CaDe^2(3\langle U \rangle/2)^3), \\ x^l &\stackrel{def}{=} \frac{\langle u_2^l \rangle}{\langle u_1^l \rangle}, \quad y^l \stackrel{def}{=} \frac{2u_{2,y}^l(1)-(1-\frac{2}{3}R_\lambda^l \hat{k})}{2u_{1,y}^l(1)-1}, \\ z^l &\stackrel{def}{=} \frac{2u_{1,y}^l(1)-1}{\langle u_1^l \rangle}, \quad M^l \stackrel{def}{=} 1 - \frac{2}{3}R_\lambda^l \hat{k}, \\ x^r &\stackrel{def}{=} \frac{\langle u_2^r \rangle}{\langle u_1^r \rangle}, \quad y^r \stackrel{def}{=} \frac{2u_{2,y}^r(1)-(1+\frac{2}{3}R_\lambda^r \hat{k})}{2u_{1,y}^r(1)-1}, \\ z^r &\stackrel{def}{=} \frac{2u_{1,y}^r(1)-1}{\langle u_1^r \rangle}, \quad M^r \stackrel{def}{=} 1 + \frac{2}{3}R_\lambda^r \hat{k}. \end{aligned} \right\} \quad (32)$$

Since $R_\lambda^l + R_\lambda^r = 1$ with $R_\lambda^l, R_\lambda^r \in (0, 1)$, we may define $\llbracket R_\lambda \rrbracket = R_\lambda^r - R_\lambda^l$ for $\llbracket R_\lambda \rrbracket \in (-1, 1)$ so that $R_\lambda^l = (1 - \llbracket R_\lambda \rrbracket)/2$ and $R_\lambda^r = (1 + \llbracket R_\lambda \rrbracket)/2$. Similarly, we have $R_\eta^l = (1 - \llbracket R_\eta \rrbracket)/2$ and $R_\eta^r = (1 + \llbracket R_\eta \rrbracket)/2$ for $\llbracket R_\eta \rrbracket \in (-1, 1)$. Recall x^l, y^l, z^l are functions of $R_\lambda^l \hat{k}$, and x^r, y^r, z^r are functions of $R_\lambda^r \hat{k}$. As a result, (31) is of form

$$\mathcal{F}(\hat{\mu}, \hat{k}, \llbracket R_\eta \rrbracket, \llbracket R_\lambda \rrbracket, \beta) = 0. \quad (33)$$

Solving (33) for $\hat{\mu}$ gives the so-called dispersion relation, which as we will see later, are multi-valued. The stability criterion is given by the region in the parameter space $(\hat{k}, \llbracket R_\eta \rrbracket, \llbracket R_\lambda \rrbracket, \beta)$ over which all solution branches have negative real parts.

In dimensional terms, the modified wavenumber \hat{k} given by (25) and the composite parameter β given by (32)₂ reads

$$\hat{k} = 3\bar{\lambda}\langle U^* \rangle |k^*|/2, \quad \beta = 8\gamma b^2/(27\bar{\eta}\bar{\lambda}^2 \langle U^* \rangle^3), \quad (34)$$

where $\langle U^* \rangle$ is the dimensional flow speed, and $|k^*|$ is the dimensional wavenumber of the disturbance. In a given experiment, $\gamma b^2/(\bar{\eta}\bar{\lambda}^2)$ is fixed a priori therefore the size of β is essentially determined by the flow speed $\langle U^* \rangle$. The remaining two parameters $(\llbracket R_\eta \rrbracket, \llbracket R_\lambda \rrbracket)$ belong to $(-1, 1) \times (-1, 1)$ by definition, where physical meaning of various parts of this square region is explained in figure 2. The special cases of Newtonian displacing UCM (top edge of figure 2) and Air displacing UCM (top right corner) have been investigated in [20]. We consider the following cases

- §5.1: UCM displacing Air (bottom left corner of figure 2).
- §5.2: UCM displacing Newtonian (bottom edge of figure 2).
- §5.3: UCM displacing UCM (interior pts. of figure 2).

Remark: It is not difficult to see from (23) and (24) that \hat{u}^l is singular if $\hat{k} = \alpha_j/R_\lambda^l$, and \hat{u}^r is singular if $\hat{k} = \alpha_j/R_\lambda^r$, where $\{\alpha_j\}_{j=1}^\infty \approx \{2, 5, 8, \dots\}$ is the set of zeros of $J_{-1/4}$. When the (modified) wavenumber \hat{k} is near any member of the set $\{\alpha_j/R_\lambda^l, \alpha_j/R_\lambda^r\}_{j=1}^\infty$, perturbations become very large, therefore the dynamics can not be

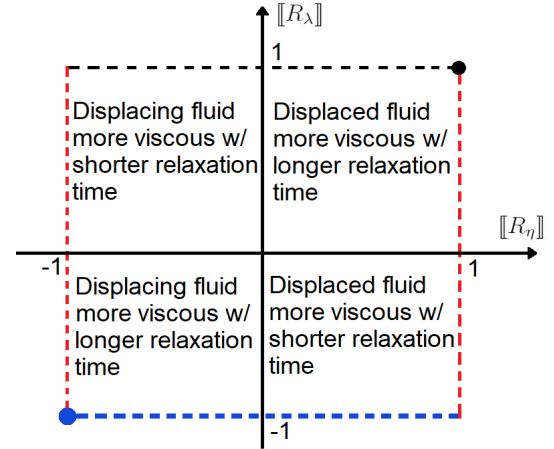


Figure 2: • : air displacing UCM. ---: Newtonian displacing UCM. • : UCM displacing air. ---: UCM displacing Newtonian. ---: not physically relevant as they all involve an inviscid UCM fluid.

captured by linear theory. By (34)₁, $R_\lambda^l := \lambda^l/\bar{\lambda}$ and $R_\lambda^r := \lambda^r/\bar{\lambda}$, the set of singular (dimensional) wavelengths is $\{3\lambda^l\langle U^* \rangle/(2\alpha_j), 3\lambda^r\langle U^* \rangle/(2\alpha_j)\}_{j=1}^\infty$, thus such singular behavior is a result of elastic effect. It should be noted that all these singular waves are removable singularities for equation (33) because all zeros of $J_{-1/4}$ are simple. On the other hand, most of such singular waves, if not all, can be neglected because of a more fundamental limitation of the theory. The Hele-Shaw scaling $L \gg b$ does not apply in the immediate vicinity of the interface where a fully three dimensional flow is expected, thus the theory becomes unreliable when the (dimensional) wavelength $1/|k^*|$ of disturbances is comparable or smaller than the thickness of this region which is expected to be $O(b)$ [38]. Recall (34)₁, the condition $1/|k^*| \gg b$ gives $\hat{k} \ll 3\bar{\lambda}\langle U^* \rangle/(2b)$. In a typical Hele-Shaw experiment, the right hand side of the last inequality is $O(10)$, therefore we restrict to $\hat{k} \in (0, 4)$ for the remainder of the development.

5.1. UCM displacing Air

This special case is obtained by taking the limits $R_\eta^l, R_\lambda^l \rightarrow 1$ and $R_\eta^r, R_\lambda^r \rightarrow 0$ in (31), which in turn reduces to ('ua' stands for UCM and Air) $\mathcal{F}^{ua} = \sum_{j=0}^2 \hat{\mu}^j f_j^{ua}(\hat{k}, \beta) = 0$ and the coefficients f_j^{ua} s are given in Appendix.A. Denote by $\hat{\mu}_j^{ua} = \hat{\mu}_j^{ua}(\hat{k}, \beta)$ for $j = 1, 2$ the two roots of \mathcal{F}^{ua} , and without loss of generality we assume $\Re\{\hat{\mu}_1^{ua}\} \leq \Re\{\hat{\mu}_2^{ua}\}$. In Appendix.A.1, it is shown that both roots are distinct real and

$$\{\hat{\mu}_1^{ua}, \hat{\mu}_2^{ua} < 0\} = \{\hat{k} < 3/2\}. \quad (35)$$

As an illustration, $\hat{\mu}_1^{ua}$ and $\hat{\mu}_2^{ua}$ v.s. \hat{k} in figure 3 for a few values of β .

The stresses associated with the eigenvalue $\hat{\mu}_1^{ua}$ or $\hat{\mu}_2^{ua}$ can become unbounded over some regions in $\hat{k} - \beta$ plane

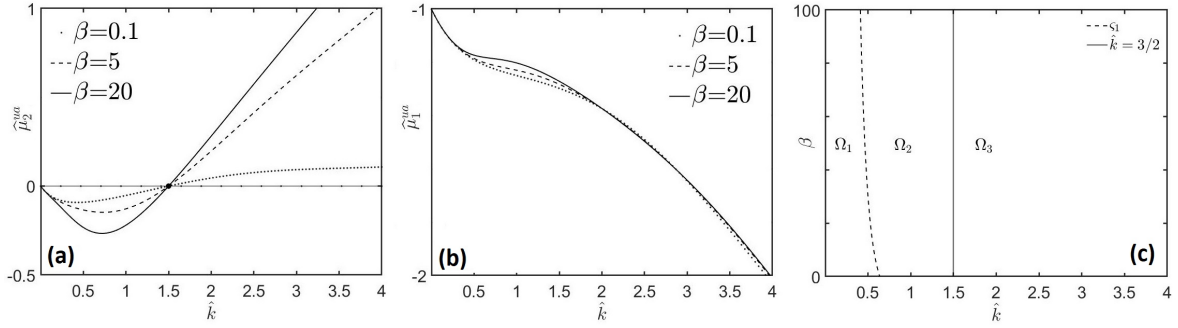


Figure 3: (a) $\hat{\mu}_2^{ua}$ are plotted v.s. \hat{k} at $\beta = 0.1, 5, 20$. (b) same is done for $\hat{\mu}_1^{ua}$. (c) the stress-singular region associated with $\hat{\mu}_1^{ua}$ and $\hat{\mu}_2^{ua}$ are respectively given by $\bar{\Omega}_2 \cup \bar{\Omega}_3$ and $\bar{\Omega}_3$. The right and left boundaries of $\bar{\Omega}_2$ are given by $\hat{k} = 3/2$ and $\beta = \zeta_1(\hat{k})$, where ζ_1 is given by (44)₂.

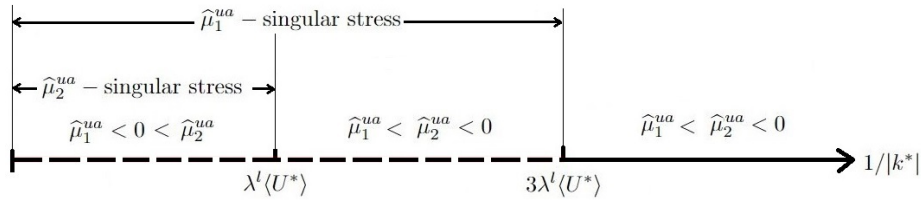


Figure 4: A summary of results of § 5.1 in terms of dimensional wavelength $1/|k^*|$.

(see Appendix.A.2 for details), and this is an elastic effect because the singularity disappears for vanishingly small relaxation time. These singular regions are shown in figure 3(c). Both modes $\hat{\mu}_1^{ua}$ and $\hat{\mu}_2^{ua}$ do not suffer from singular-stress issues for sufficiently long waves, i.e. over $\bar{\Omega}_1$. However, the stress becomes singular for both modes for short waves i.e. over $\bar{\Omega}_3$, and this can happen even for slow flow (large β). Interestingly, $\hat{\mu}_1^{ua}$ is more prone to suffer from singular stress than $\hat{\mu}_2^{ua}$ even though $\hat{\mu}_1^{ua} < \hat{\mu}_2^{ua}$.

Using (34)₁ (with $\bar{\lambda} = \lambda^l$), we may convert (35) into dimensional terms, namely $1/|k^*| > \lambda^l \langle U^* \rangle$, where $1/|k^*|$ and $\langle U^* \rangle$ are the dimensional wavelength and flow speed. Similarly, the left boundary of $\bar{\Omega}_2$ in figure 3(c) depends weakly on β and is approximately located at $\hat{k} = 1/2$, or equivalently $1/|k^*| = 3\lambda^l \langle U^* \rangle$. The summary of results obtained thus far is illustrated in figure 4. Although both eigenvalues are negative for any disturbance of wavelength $1/|k^*|$ greater than $\lambda^l \langle U^* \rangle$, one can only conclude stability for $1/|k^*| \in (3\lambda^l \langle U^* \rangle, \infty)$ because the stress becomes unbounded for at least one eigenvalues if $1/|k^*| \in (\lambda^l \langle U^* \rangle, 3\lambda^l \langle U^* \rangle)$. The size of $3\lambda^l \langle U^* \rangle$ is typically on the order of millimeter range and close to the typical gap size for a Hele-Shaw cell, thus it is consistent with the Hele-Shaw approximation $1/|k^*| \gg b$. For wavelength shorter than $3\lambda^l \langle U^* \rangle$, linear theory fails because it assumes all disturbances must be small to begin with, however it can nonetheless indicate, as $1/|k^*| \rightarrow 3\lambda^l \langle U^* \rangle$, the stress must become very large, thus establishing the connection to fracturing instability observed in experiments [25, 49, 32, 46]. This explanation should be taken with caution because it may be due to (i) a flaw of the UCM model itself, which

allows the polymer particles to be infinitely stretched due to Hook's spring law used [4, 39, 33], leading to unbounded stress, or (ii) the mathematical nature of this singular behavior is very similar to the ones found in the Rayleigh's eq. or Orr-Sommerfeld eq. in unbounded domain [13], which is associated with the continuous part of the eigen-spectrum. There appears to be no simple way to resolve this but dealing with the full initial value problem which is outside the scope of this paper.

Remark: To simplify the language for the remainder of the development, we still adopt the conventional language that 'stable' means the the real part of the largest eigenvalues is negative and 'unstable' if positive, and neutrally/marginally 'stable' if 0. The reason for this emphasis is because there can be stress singularity even when it is 'stable' as discussed above.

5.2. UCM displacing Newtonian

This special case is obtained by taking the limit $R_\lambda^r \rightarrow 0$ in (31), which in turn reduces to ('un' stands for UCM and Newtonian) $\mathcal{F}^{un} = \sum_{j=0}^3 \hat{\mu}^j f_j^{un}(\hat{k}, \llbracket R_\eta \rrbracket, \beta) = 0$ and the coefficients f_j^{un} s are given in Appendix.B. Denote by $\hat{\mu}_j^{un} = \hat{\mu}_j^{un}(\hat{k}, \llbracket R_\eta \rrbracket, \beta)$ for $j = 1, 2, 3$ the three roots of \mathcal{F}^{un} . Without loss of generality, we may assume $\Re\{\hat{\mu}_1^{un}\} \leq \Re\{\hat{\mu}_2^{un}\} \leq \Re\{\hat{\mu}_3^{un}\}$.

Since $\hat{\mu}_3^{un}$ s are polynomial roots, the condition for $\Re\{\hat{\mu}_3^{un}\} < 0$ is given by the Routh-Hurwitz criterion, from which we obtain (see Appendix.B.1 for details)

$$\{\Re\{\hat{\mu}_3^{un}\} < 0 \mid \llbracket R_\eta \rrbracket \leq 0\} = \{\hat{k} < 3/2\}, \quad (36)$$

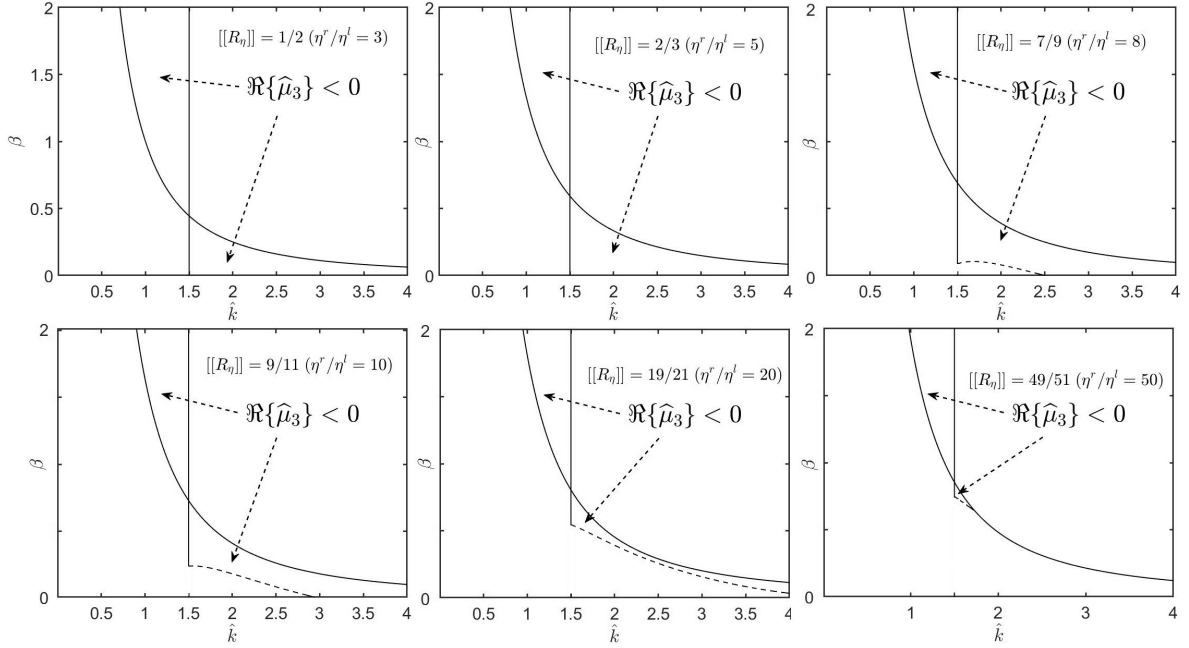


Figure 5: The region $\Re\{\hat{\mu}_3\} < 0$ described by (37) is shown in the $\hat{k} - \beta$ plane for select values of $\llbracket R_\eta \rrbracket$. The upper curve (solid) is given by $\beta = \beta_0$, which intersects with the vertical line at $(\hat{k}, \beta) = (3/2, 8\llbracket R_\eta \rrbracket/9)$. The dashed curve is $\beta = \beta_2$. The $\Re\{\hat{\mu}_3\} < 0$ branch right to the vertical line vanishes in the limit $\llbracket R_\eta \rrbracket \rightarrow 1$.

and

$$\{\Re\{\hat{\mu}_3\} < 0 \mid \llbracket R_\eta \rrbracket > 0\} \\ = \{\beta > \beta_0 \mid \hat{k} < 3/2\} \cup \{\beta_2 < \beta < \beta_0 \mid \hat{k} > 3/2\}, \quad (37)$$

where β_0 and β_2 are functions of \hat{k} and $\llbracket R_\eta \rrbracket$ and given by (52)₁ and (55)₂ respectively. In figure 5, the region described in (37) is shown in the $\hat{k} - \beta$ plane for select values of $\llbracket R_\eta \rrbracket > 0$.

Viscous effect is still the dominant mechanism in determining stability for long waves (stable if $\llbracket R_\eta \rrbracket \leq 0$, or equivalently $\eta^r/\eta^l \leq 1$). Increasing β (slow flow) has a stabilizing effect on long waves. Unlike the Saffman-Taylor case (Newtonian displacing Newtonian) where the short waves are stabilized by interfacial tension, the short waves are destabilized by elastic effect. On the other hand, similar to the special case discussed in §5.1, the stress associated with $\hat{\mu}_j^{un}$ can become unbounded due to elastic effect over some regions in the $\hat{k} - \beta$ plane, which are dependent on the viscosity contrast parameter $\llbracket R_\eta \rrbracket \in (-1, 1)$. We find that long waves do not suffer from such singular behavior but short waves always do. In particular (see Appendix B.2 for details), for $\llbracket R_\eta \rrbracket \lesssim 1/2$ ($\eta^r/\eta^l \lesssim 3$), we find (i) $\hat{\mu}_1^{un}$ is never stress-singular, and (ii) $\hat{\mu}_3^{un}$ is stress-singular for $\hat{k} > 3/2$, and (iii) $\hat{\mu}_2^{un}$ is stress-singular if $\hat{k} > \hat{k}_*(\beta, \llbracket R_\eta \rrbracket)$. Further, \hat{k}_* depends on $\llbracket R_\eta \rrbracket$ and β weakly, and for reasonable β values (upto 100), \hat{k}_* is approximately 1/2. In summary, the stress-singular regions for $\hat{\mu}_1^{un}$ and $\hat{\mu}_3^{un}$ are contained in that of $\hat{\mu}_2^{un}$. For larger $\llbracket R_\eta \rrbracket$, this remains to be the case unless for relatively small β (fast flow).

5.3. UCM displacing UCM

After some algebra, (31) can be rewritten as $\mathcal{F} = \sum_{j=0}^4 \hat{\mu}^j f_j(\hat{k}, \llbracket R_\eta \rrbracket, \llbracket R_\lambda \rrbracket, \beta) = 0$, and the coefficients f_j s are given in Appendix.C. Denote by $\hat{\mu}_j = \hat{\mu}_j(\hat{k}, \llbracket R_\eta \rrbracket, \llbracket R_\lambda \rrbracket, \beta)$ for $j = 1, 2, 3, 4$ the four roots of \mathcal{F} . Without loss of generality, we assume $\Re\{\hat{\mu}_1\} \leq \Re\{\hat{\mu}_2\} \leq \Re\{\hat{\mu}_3\} \leq \Re\{\hat{\mu}_4\}$.

It is shown in Appendix.C.1 that viscous effect is still the dominant mechanism in determining stability for long waves, namely $\Re\{\hat{\mu}_4\} < 0$ for small \hat{k} if and only if $\llbracket R_\eta \rrbracket \leq 0$. For \hat{k} bounded away from 0, we first consider the case where the displacing fluid more or equally viscous, i.e. $\llbracket R_\eta \rrbracket \leq 0$. In Appendix.C.2, it is shown

$$\{\Re\{\hat{\mu}_4\} < 0\} = \{\hat{k} < \hat{k}_*\}, \quad \text{where } \hat{k}_* \stackrel{def}{=} 3/(2R_\lambda^l). \quad (38)$$

The plot of $\Re\{\hat{\mu}_4\}$ v.s \hat{k} is shown in figure 6 for several combinations of $\llbracket R_\eta \rrbracket$, $\llbracket R_\lambda \rrbracket$ and β . By (34)₁ and $R_\lambda^l := \lambda^l/\bar{\lambda}$, $\hat{k} > \hat{k}_*$ is equivalent to $1/|k^*| < \lambda^l \langle U^* \rangle$ from which we conclude (i) the flow becomes unstable when the wavelength is shorter than the distance traveled by the fluid bulk within one relaxation time of the displacing fluid, and (ii) decreasing the relaxation time of the displacing fluid or the flow speed has a stabilizing effect. Since this is true for all $\llbracket R_\eta \rrbracket \leq 0$, elastic effect of the displacing fluid plays the decisive role (along with the flow speed) in causing short wave instability. This remains to be the case for $\llbracket R_\eta \rrbracket > 0$.

Now we consider the case where the displaced fluid is more viscous, namely $\llbracket R_\eta \rrbracket > 0$. There can arise a third kind of singular behavior in such case. It is shown in Appendix.C.3 that if the parameter combination $(\llbracket R_\eta \rrbracket, \llbracket R_\lambda \rrbracket, \beta)$

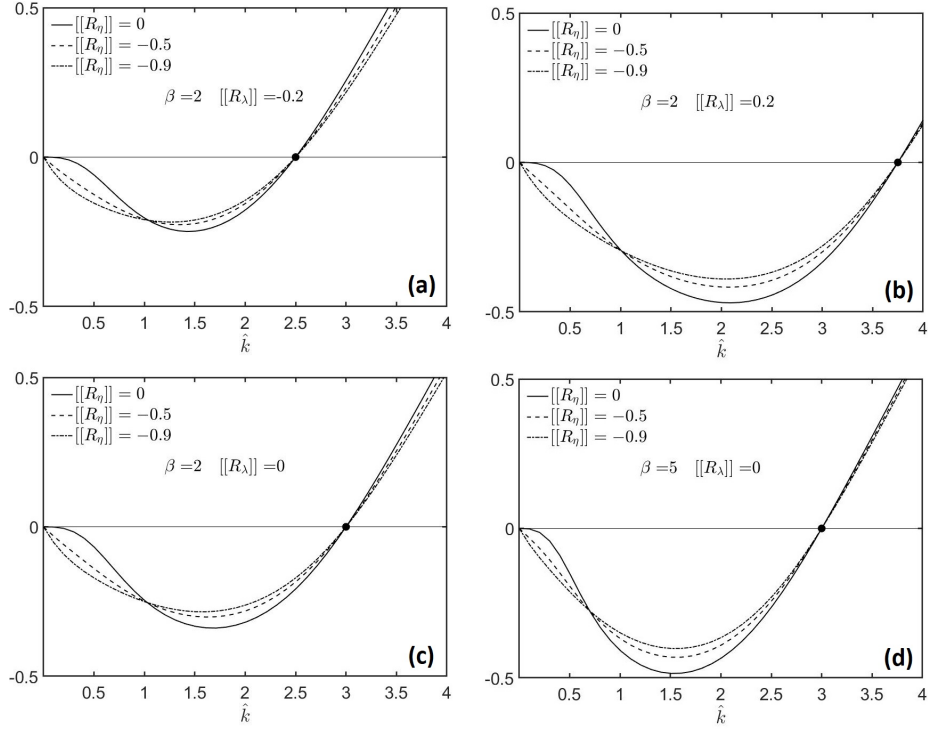


Figure 6: (a) $\Re\{\hat{\mu}_4\}$ v.s. \hat{k} at $\llbracket R_\eta \rrbracket = 0, -0.5, -0.9$ with fixed $\beta = 2$ and $\llbracket R_\lambda \rrbracket = -0.2$. The solid dot is located at $\hat{k} = 3/(2R_\lambda^l)$, beyond which the flow becomes unstable. (b)-(d) the same are done with different values of β and $\llbracket R_\lambda \rrbracket$.

falls on or below the graph of

$$\beta_*(\llbracket R_\eta \rrbracket, \llbracket R_\lambda \rrbracket) \stackrel{def}{=} \max_{\hat{k}} \zeta(\hat{k}, \llbracket R_\eta \rrbracket, \llbracket R_\lambda \rrbracket)$$

where ζ is given by (63), then there exists $\hat{k} = \hat{k}_*$ at which $\hat{\mu}_4$ diverges to $+\infty$. The graph of β_* is shown in figure 7(a). The contour $\beta_* = 0$ is shown in figure 7(b). A few axis-parallel curves along the surface is shown in figure 7(c),(d). We call such phenomenon a resonance because the largest eigenvalue increases very sharply near certain $\hat{k} = \hat{k}_*$, which we shall call a (modified) resonating wavenumber. The supremum of β_* is approximately 1.113 obtained in the limit $\llbracket R_\eta \rrbracket, \llbracket R_\lambda \rrbracket \rightarrow 1$. It is not surprising that this limiting value coincides with the findings in [20] because it degenerates to an air displacing UCM setting. Further, if only $\llbracket R_\lambda \rrbracket \rightarrow 1$ (Newtonian displacing UCM), the resonance also does not occur as predicted in [20]. As an illustration, we show the resonance at $(\llbracket R_\eta \rrbracket, \llbracket R_\lambda \rrbracket, \beta) = (0.9, 0, 0.11)$. In figure 8(b), $\hat{\mu} \rightarrow \infty$ at $\hat{k} \approx 2.15$ as $\beta \rightarrow 0.11$ from above with fixed $(\llbracket R_\eta \rrbracket, \llbracket R_\lambda \rrbracket) = (0.9, 0)$. For smaller β , for example $\beta = 0.05$, there will be two resonating wavenumbers, namely at $\hat{k} \approx 1.7$ and $\hat{k} \approx 3.37$ (see figure 8(a)).

The resonance can be avoided if $\llbracket R_\eta \rrbracket \lesssim 0.797$ ($\eta^r/\eta^l \lesssim 9$), or $\llbracket R_\lambda \rrbracket \lesssim -0.51$ ($\lambda^r/\lambda^l \lesssim 0.32$), or $\beta \gtrsim 1.113$. Notice that these are sufficient conditions but not necessary. For example, if $\llbracket R_\eta \rrbracket = 0.9$ ($\eta^r/\eta^l \approx 19$), then the resonance can be avoided for all $\beta > 0$ as long as $\llbracket R_\lambda \rrbracket \lesssim -0.389$ ($\lambda^r/\lambda^l \lesssim 0.44$) or $\llbracket R_\lambda \rrbracket \gtrsim 0.847$ ($\lambda^r/\lambda^l \gtrsim 12$) (see figure 7(b)). If these ranges of relaxation time combinations

are not available for an experiment, say only $\llbracket R_\lambda \rrbracket = 0$ ($\lambda^r/\lambda^l = 1$) is available, then the resonance can still be avoided by keeping $\beta > \beta_* \approx 0.11$. By (34)₂, $\beta > \beta_*$ is equivalent to $\langle U^* \rangle < (8\gamma b^2/(27\eta\lambda^2))^{1/3}/\beta_*^{1/3}$, the resonance can always be avoided by keeping the flow to be sufficiently slow (the quantity inside the parenthesis is fixed for any given experiment and the value of β_* can be computed numerically (see figure 7(c),(d)).

For $\beta > 1.113$ so no resonance occurs for all $\llbracket R_\eta \rrbracket, \llbracket R_\lambda \rrbracket \in (-1, 1)$. It is shown in Appendix.C.3.2 that

$$\left. \begin{aligned} \{\Re\{\hat{\mu}_4\} < 0\} &= \{\hat{k}_o < \hat{k} < \hat{k}_*\}, \\ \hat{k}_* &\stackrel{def}{=} 3/(2R_\lambda^l), \quad \hat{k}_o \stackrel{def}{=} (2\llbracket R_\eta \rrbracket/\beta)^{1/2}. \end{aligned} \right\} \quad (39)$$

Over the unstable long waveband $\hat{k} < \hat{k}_o$, $\Re\{\hat{\mu}_4\}$ attains a maximum $\hat{\mu}_\dagger$ at some $\hat{k} = \hat{k}_\dagger$ (see figure 9-11). We find both $\hat{\mu}_\dagger$ and \hat{k}_\dagger decrease if $\llbracket R_\eta \rrbracket$ decreases, or $\llbracket R_\lambda \rrbracket$ decreases, or β increases. Since \hat{k}_o shifts to the left as $\llbracket R_\eta \rrbracket$ decreases or β increases, changing these two parameters in such fashion does not only make the unstable long wave less unstable (slower growth) but also has a stabilizing effect. Over the unstable short waveband $\hat{k} > \hat{k}_*$, $\Re\{\hat{\mu}_4\}$ increases as \hat{k} . $\llbracket R_\eta \rrbracket$ and β have rather weak effects on $\Re\{\hat{\mu}_4\}$ (see figure 9). Increasing $\llbracket R_\lambda \rrbracket$ has a more significant effect on $\Re\{\hat{\mu}_4\}$ (see figure 10) and can stabilize certain unstable short waves (\hat{k}_* shifts to the right).

At last, similar to the special case of UCM displacing air (§5.1) and UCM displacing Newtonian (§5.2), the stress

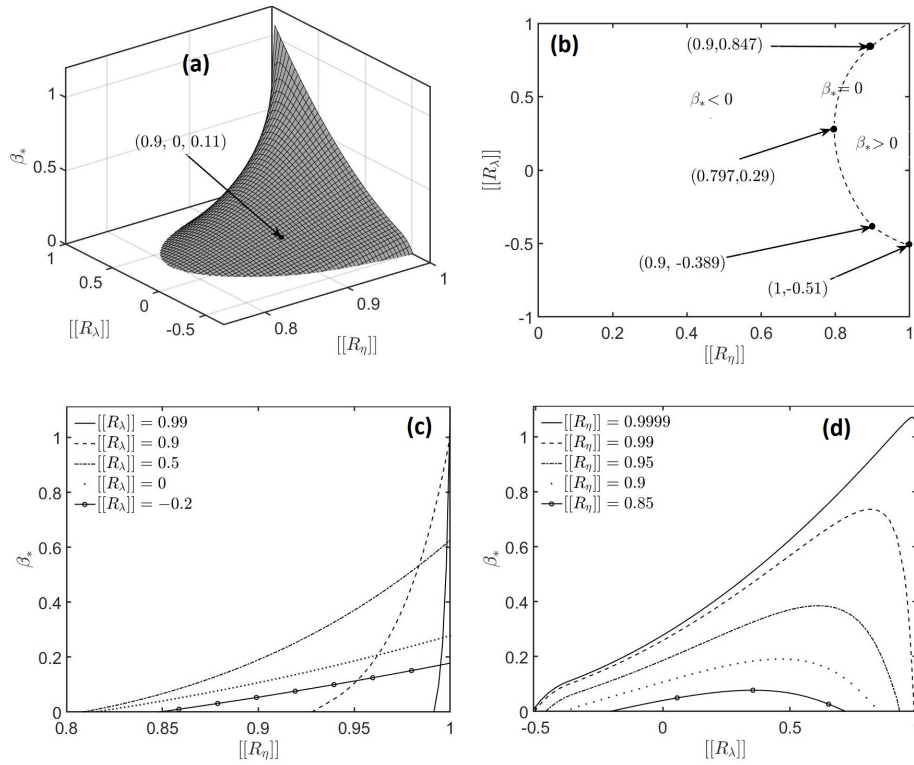


Figure 7: (a): The graph of $\beta_*(\llbracket R_\eta \rrbracket, \llbracket R_\lambda \rrbracket)$. Resonance occurs when $(\llbracket R_\eta \rrbracket, \llbracket R_\lambda \rrbracket, \beta)$ belongs to the (closed) volume region bounded below by the graph. (b): If $(\llbracket R_\eta \rrbracket, \llbracket R_\lambda \rrbracket)$ falls inside the region right to the dashed curve given by $\beta_* = 0$, the resonance can be avoided by taking $\beta > \beta_*$. For example, any $\beta > \beta_* \approx 0.11$ suffices for $(\llbracket R_\eta \rrbracket, \llbracket R_\lambda \rrbracket) = (0.9, 0)$. (c) and (d): Several curves along the surface given in (a) are shown.

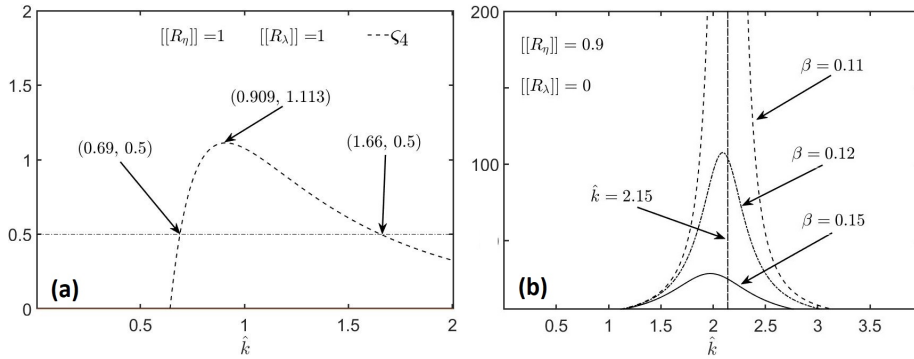


Figure 8: (a): ζ v.s. \hat{k} at fixed $(\llbracket R_\eta \rrbracket, \llbracket R_\lambda \rrbracket) = (0.9, 0)$. The resonance occurs over the curve $\beta = \zeta$. For example, if $\beta \approx 0.11$, the resonance occurs at $\hat{k} \approx 2.15$. This is illustrated in (b), $\hat{\mu}_4 \rightarrow \infty$ at $\hat{k} \approx 2.15$ as $\beta \rightarrow 0.11$ from above. For smaller β , the singularity will split into two (at $\hat{k} \approx 1.7$ and $\hat{k} \approx 3.37$ for $\beta \approx 0.05$).

associated to $\hat{\mu}_j$ can come singular. For each $j = 1, 2, 3, 4$, it is given by some some regions in $\hat{k} - \beta$ plane whose boundaries depend on $\llbracket R_\eta \rrbracket$ and $\llbracket R_\lambda \rrbracket$. Due to the complexity of the roots, no expressions for the boundary curves are obtained. As a general trend, we find short waves always suffer from such singular behavior and long waves do not. This is illustrated for some select combinations of $\llbracket R_\eta \rrbracket$ and $\llbracket R_\lambda \rrbracket$ in appendix §C.4.

6. Conclusions

In [20], the role of elasticity on the formation of fingering instability is studied in a rectilinear Hele-Shaw cell where an UCM fluid is displaced by a Newtonian fluid. Bearing the same purpose, this article further generalizes the previous results by replacing the Newtonian fluid by another UCM fluid. A set of reduced equations is first derived in the thin gap limit through a proper scaling scheme. These equations are then linearized about the steady state unidirectional flow and the method of normal mode is then employed, which

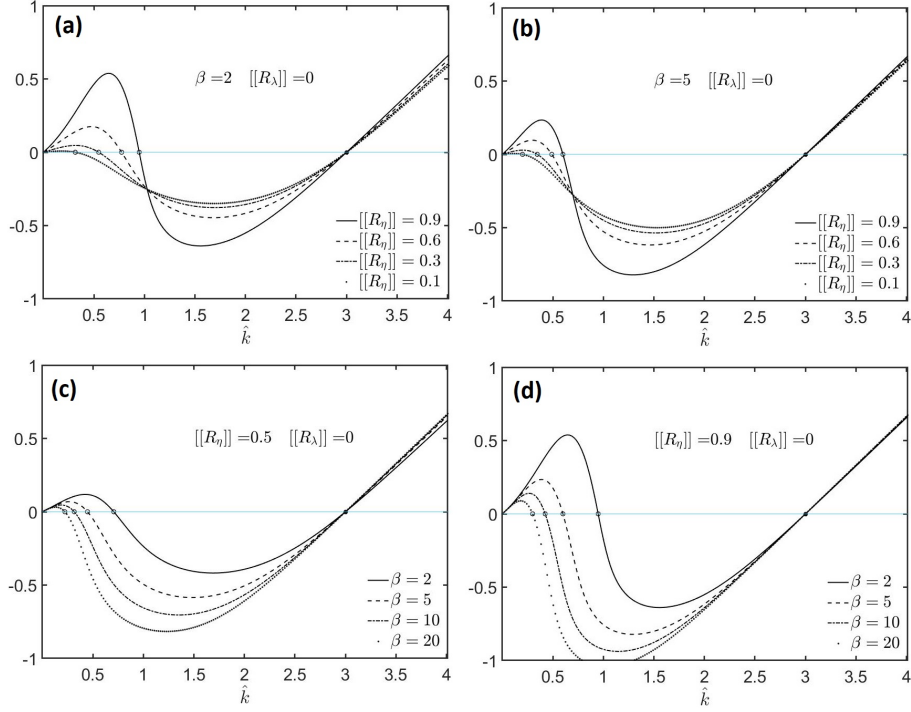


Figure 9: (a), (b): $\Re\{\hat{\mu}_4\}$ v.s. \hat{k} with fixed β and $\llbracket R_\lambda \rrbracket$. The solid dots $\hat{k} = \hat{k}_*$ and the empty circles $\hat{k} = \hat{k}_0$ are given by (39). (c), (d): same are done for fixed $\llbracket R_\eta \rrbracket$ and $\llbracket R_\lambda \rrbracket$.

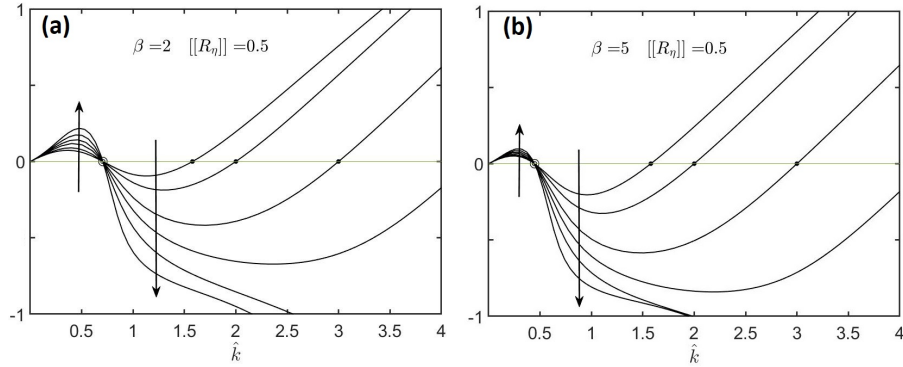


Figure 10: (a): $\Re\{\hat{\mu}_4\}$ v.s. \hat{k} with fixed $\beta = 2$ and $\llbracket R_\eta \rrbracket = 0.5$. As $\llbracket R_\lambda \rrbracket$ increases from -0.9 to 0.9 , the curve moves in direction of the arrow. The solid dots $\hat{k} = \hat{k}_*$ and the empty circles $\hat{k} = \hat{k}_0$ are given by (39). (b): the same is done with $\beta = 5$.

in turn leads to an eigenvalue relation in the form of a quartic equation with the temporal growth rate given by the roots of the quartic polynomial. In the special case of UCM displacing air or viscous Newtonian, the polynomial becomes quadratic or cubic respectively.

The elastic effect of the displacing layer always has a destabilizing effect and can introduce additional singularities. In the classical Saffman-Taylor case, the flow is stable to small disturbances of all wavelengths if and only if $\eta^r/\eta^l \leq 1$. If $\eta^r/\eta^l > 1$, long waves become unstable but short waves are stabilized due to interfacial tension effect. In our study, viscous effect is still the dominant mechanism in determining the long wave stability (stable if $\eta^r/\eta^l \leq 1$). However, the short waves are always unstable (wavelength

shorter than $\lambda^l \langle U^* \rangle$). This is a result of elastic effect because it happens for all values of η^r/η^l , and interfacial tension does not remove this instability. The simplest physical explanation for this destabilizing effect is that the fluids do not have sufficient time to fully relax ($De \sim O(1)$) to dissipate the elastic energy stored over a short length scale, which is then transferred to the interface thus creating additional instability on top of the usual fingering instability induced by viscosity contrasts. In addition, short wave disturbances also suffer from up to three types singular behaviors described in (i)-(iii) below, all of which are associated with elastic effects. It should be noted such singular behaviors are also found in [20], but the newly introduced elasticity of the displacing layer has significant effect on where they happen.

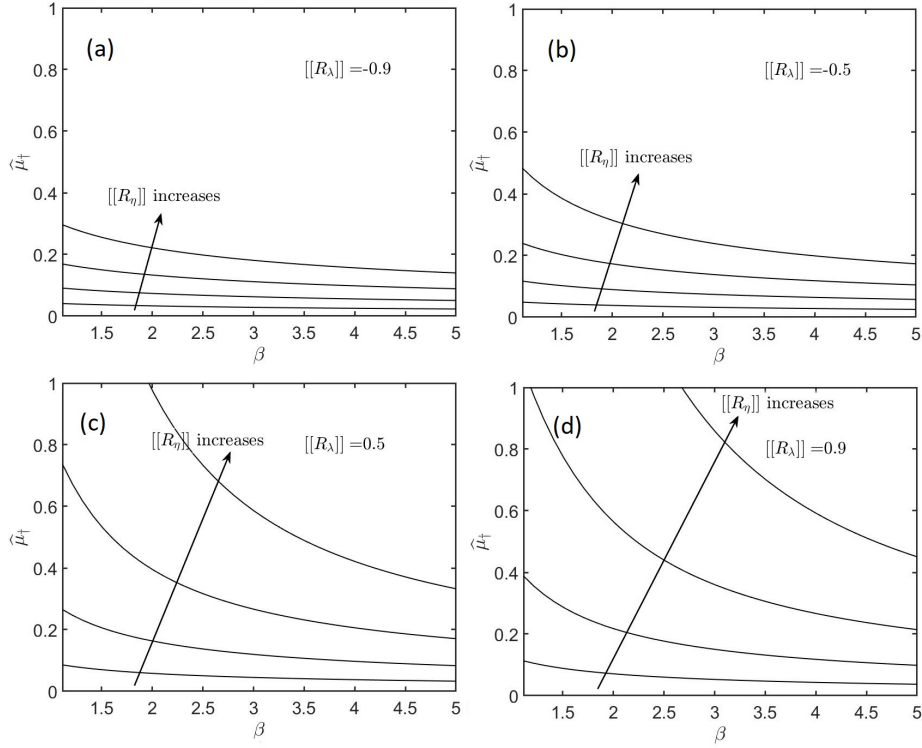


Figure 11: (a): $\hat{\mu}_+$ v.s. β at $[[R_\eta]] = 0.3, 0.5, 0.7, 0.9$ are shown with fixed $[[R_\lambda]] = -0.9$. (b),(c),(d): same are done for $[[R_\lambda]] = -0.5, 0.5, 0.9$ respectively.

1. There exists infinitely many isolated wavenumbers at which the velocity disturbance becomes unbounded. The wavelengths of such singular waves are proportional to $\lambda^l \langle U^* \rangle$ or $\lambda^r \langle U^* \rangle$, and all are contained in the interval $(0, 3 \max\{\lambda^l, \lambda^r\} \langle U^* \rangle / 4)$. For a typical Hele-Shaw flow experiment, these singular wavelengths are on the order of a millimeter or less.
2. The temporal growth rate can be unbounded at certain wavenumbers if the η^r / η^l and the λ^r / λ^l fall within a certain range. This singular behavior strongly resembles a resonance phenomenon, however it can always be avoided by keeping the flow sufficiently slow.
3. The stress becomes unbounded for short waves, which can happen even for slow flow. The mathematical origin of this is similar in nature to the one found in Rayleigh's eq. or Orr-Sommerfeld eq. in unbounded domain [13], which is associated with the continuous part of the eigen-spectrum. Considering the full initial value problem may be necessary to resolve such issues but this is beyond the scope of this paper however we are making effort on this direction. Another possible reason is that this is simply a flaw of the UCM model. In its equivalent microscopic description, the polymer particles are treated as Hookean dumbbells, which can be infinitely stretched producing singular stress. Although UCM model does not take into account the Newtonian part of the stress contributed by the solvent which is expected to have certain regularizing effect,

our preliminary findings show the singularity remains even when the Oldroyd-B model is used instead.

The analysis of this paper shows the formidable mathematical challenges that Hele-Shaw flows involving simplest type of viscoelastic fluids, namely UCM, pose and how to overcome these to extract relevant information about these flows. Different types of singularities lurking in these flows are strongly associated with elasticity, some of which could be precursors to singular physical phenomena. In particular, it quite well known in solid mechanics that large stress can lead to fractures. For the Deborah regime $O(1)$ considered here, the fluid becomes more solid-like from which singular stress is predicted by the analysis. Although linear theory cannot predict how such singular behavior will evolve, it can nonetheless indicate the stress will become very large near the singular parameter regions. As a result, we believe this has strong connection to the fractures observed in experiments [25, 49, 32, 46].

This paper sets the foundation for solving Hele-Shaw type flows involving more realistic fluids such as Oldroyd-B and fluids with other non-Newtonian properties. The analysis perhaps could be generalized to other industrially relevant flows within a thin domain. Finally, we mention some future directions in this area that one can undertake. Extending the analysis of this paper from UCM to Oldroyd-B fluid is of practical interest. The next natural step up is to consider a radial geometry. Many more interesting but certainly more challenging problems can be considered such as including more non-Newtonian properties, wetting effects, effect of

secondary flows near the interface, time dependent injection rate, variable gap size, flexible walls, or perhaps even with curvatures in the lateral direction, etc. We have mentioned here just a few possibilities and readers should be able to envision many other directions in this area.

7. Acknowledgements

It is a pleasure to thank two anonymous reviewers whose comments have helped us improve the paper significantly. Financial support from departmental graduate office to the author ZH and from the U.S. National Science Foundation through grant DMS-1522782 to the author PD is gratefully acknowledged.

A. UCM displacing Air

In the limits $R_\eta^l, R_\lambda^l \rightarrow 1$ and $R_\eta^r, R_\lambda^r \rightarrow 0$, (31) reduces to (x^l, y^l, z^l are now evaluated at $R_\lambda^l = 1$)

$$\frac{\hat{\mu}z^l(\hat{\mu} + y^l)}{(\hat{\mu} + 1 - 2\hat{k}/3)(\hat{\mu} + x^l)} = \beta\hat{k}^3 + 2\hat{k}. \quad (40)$$

After some algebra, (40) can be written as ('ua' stands for UCM and Air) $\mathcal{F}^{ua} = \sum_{j=0}^2 \hat{\mu}^j f_j^{ua}(\hat{k}, \beta) = 0$, where

$$\left. \begin{aligned} f_2^{ua} &= s - z^l, & f_1^{ua} &= s(M^l + x^l) - y^l z^l, \\ f_0^{ua} &= sM^l x^l, & s &= \beta\hat{k}^3 + 2\hat{k}, \\ \beta &= 1/(CaDe^2(3\langle U \rangle/2)^3), & M^l &= 1 - 2\hat{k}/3. \end{aligned} \right\} \quad (41)$$

Let $\hat{\mu}_j^{ua} = \hat{\mu}_j^{ua}(\hat{k}, \beta)$ be the $j = 1, 2$ two roots of \mathcal{F}^{ua} , and without loss of generality we assume $\Re\{\hat{\mu}_1^{ua}\} \leq \Re\{\hat{\mu}_2^{ua}\}$. The following inequalities (numerically obtained) are important to later development

$$\left. \begin{aligned} z^l &< -3, & 1 &< x^l, y^l, \\ |M^l| &< x^l, y^l, & x^l &< M^l + \hat{k}. \\ z^l &\rightarrow -3, & x^l, y^l &\rightarrow 1, \text{ as } \hat{k} \rightarrow 0. \end{aligned} \right\} \quad (42)$$

A.1. Stable waveband

By definition, the discriminant of \mathcal{F}^{ua} is given by $\Delta = s^2(M^l - x^l)^2 - 2z^l((M^l + x^l)y^l - 2M^l x^l)s + (y^l z^l)^2$. Numerical result show $0 < (M^l + x^l)y^l - 2M^l x^l$, thus $\Delta > 0$ because $z^l < 0 < s$. As a result, $\hat{\mu}_1^{ua}$ and $\hat{\mu}_2^{ua}$ are distinct real. Since $f_2^{ua}, f_1^{ua} > 0$ by (42), it must be $\hat{\mu}_1^{ua} < 0$. On the other hand, $\hat{\mu}_2^{ua} < 0$ if and only if $f_0^{ua} > 0$, which is true if and only if $M^l > 0$, or equivalently $\{\hat{\mu}_2^{ua} < 0\} = \{\hat{k} < 3/2\}$.

A.2. Stress singularity

It is clear from the beginning part of §5 that $\tilde{\tau}^{xx,l}$ is assumed a priori to be integrable across the cell gap $y \in (-1, 1)$. This requires ψ^l given by (23)₄ (with $R_\lambda^l = 1$) to be

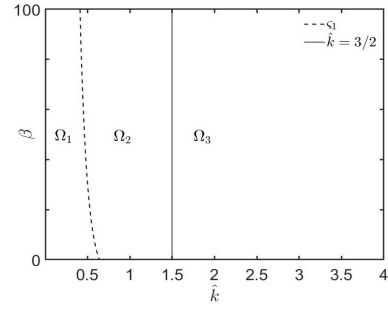


Figure 12: In $\hat{k} - \beta$ plane, the region where $\mathcal{F}^{ua}(-M^l - \hat{k}) < 0$ is labeled Ω_1 with boundary curve (dashed) $\partial\Omega_1 = \{\beta = \varsigma_1(\hat{k})\}$, and $\mathcal{F}^{ua}(-M^l) > 0$ over Ω_3 with boundary curve (solid) $\partial\Omega_3 = \{\hat{k} = 3/2\}$. Over $\bar{\Omega}_2 \cup \bar{\Omega}_3$, $0 \leq \mathcal{F}^{ua}(-M^l - \hat{k})$. Over $\bar{\Omega}_1 \cup \bar{\Omega}_2$, $\mathcal{F}^{ua}(-M^l) < 0$.

non-zero over $y \in [-1, 1]$, which true if and only if (with $R_\lambda^l = 1$)

$$\hat{\mu} \notin I, \quad I \stackrel{def}{=} [-M^l - \hat{k}, -M^l]. \quad (43)$$

In other words, if $\hat{\mu} = \hat{\mu}_j^{ua}$ does not satisfy (43), then the stress associated with $\hat{\mu}_j^{ua}$ is singular. To see this is an elastic effect, we may express (43) in dimensional forms (superscript *) $\mu^* \notin [-|k^*|\langle U^* \rangle/2 - 1/\lambda^l, |k^*|\langle U^* \rangle - 1/\lambda^l]$, which is satisfied for any finite μ^* for sufficiently small λ^l . It can be shown using definition and (42) that

$$\left. \begin{aligned} \{\mathcal{F}^{ua}(-M^l - \hat{k}) < 0\} &= \{\beta < \varsigma_1(\hat{k})\}, \\ \varsigma_1 &\stackrel{def}{=} \frac{z^l}{\hat{k}^3} \frac{M^l + \hat{k}}{\hat{k}} \frac{M^l + \hat{k} - y^l}{M^l + \hat{k} - x^l} - \frac{2}{\hat{k}^2}, \end{aligned} \right\} \quad (44)$$

and

$$\{0 < \mathcal{F}^{ua}(-M^l)\} = \{\hat{k} > 3/2\}. \quad (45)$$

The sets described by (44) and (45) are some regions in $\hat{k} - \beta$ plane, denoted by Ω_1 and Ω_3 (both open) respectively with boundary $\partial\Omega_1 = \{\beta = \varsigma_1\}$ and $\partial\Omega_3 = \{\hat{k} = 3/2\}$. In figure 12, Ω_1 and Ω_3 are shown. Since $\hat{\mu}_1^{ua}$ and $\hat{\mu}_2^{ua}$ are always real and $\hat{\mu}_1^{ua} < \hat{\mu}_2^{ua}$, there are four possibilities: only one, both, or neither of $\hat{\mu}_j^{ua}$ belongs to the interval I . In particular

(i) $\hat{\mu}_1^{ua} \notin I$ and $\hat{\mu}_2^{ua} \in I$. In other words, only the larger root of \mathcal{F}^{ua} is contained in the interval I , which is true if and only if $\mathcal{F}^{ua}(-M^l - \hat{k}) \leq 0 \leq \mathcal{F}^{ua}(-M^l)$, or equivalently $\bar{\Omega}_1 \cap \bar{\Omega}_3$. But this is empty as the two regions are disjoint, as a result $\{\hat{\mu}_1^{ua} \notin I\} \cap \{\hat{\mu}_2^{ua} \in I\} = \emptyset$.

(ii) $\hat{\mu}_1^{ua} \in I$ and $\hat{\mu}_2^{ua} \notin I$. This is true if and only if $\mathcal{F}^{ua}(-M^l - \hat{k}) \geq 0 \geq \mathcal{F}^{ua}(-M^l)$, or equivalently $\{\bar{\Omega}_2 \cup \bar{\Omega}_3\} \cap \{\bar{\Omega}_1 \cup \bar{\Omega}_2\} = \{\bar{\Omega}_2\}$. As a result $\{\hat{\mu}_1^{ua} \in I\} \cap \{\hat{\mu}_2^{ua} \notin I\} = \{\bar{\Omega}_2\}$.

(iii) $\hat{\mu}_1^{ua}, \hat{\mu}_2^{ua} \in I$. This can only happen for $\mathcal{F}^{ua}(-M^l - \hat{k}) \geq$

0 and $\mathcal{F}^{ua}(-M^l) \geq 0$ (i.e. $\overline{\Omega}_3$). This is also sufficient because $-M^l - \hat{k}$ is always negative, and $\hat{\mu}_2^{ua} \geq 0$ over Ω_3 so that $-M^l - \hat{k} < \hat{\mu}_2^{ua}$. In addition, $\hat{\mu}_1$ is always negative, and $-M^l \geq 0$ over $\overline{\Omega}_3$ so that $\hat{\mu}_1^{ua} < -M^l$. The case $\hat{\mu}_1^{ua} \leq -M - \hat{k} < -M^l \leq \hat{\mu}_2^{ua}$ is not possible because it would imply at least one of $\mathcal{F}^{ua}(-M^l - \hat{k})$ or $\mathcal{F}^{ua}(-M^l)$ is negative. As a result, $\{\hat{\mu}_1^{ua}, \hat{\mu}_2^{ua} \in I\} = \{\overline{\Omega}_3\}$.

(iv) $\hat{\mu}_1^{ua}, \hat{\mu}_2^{ua} \notin I$. This can be obtained through set manipulations

$$\begin{aligned} \{\hat{\mu}_1^{ua}, \hat{\mu}_2^{ua} \notin I\} &= \{\{\hat{\mu}_1^{ua} \in I\} \cup \{\hat{\mu}_2^{ua} \in I\}\}^c \\ &= \{\{\{\hat{\mu}_1^{ua}, \hat{\mu}_2^{ua} \in I\} \cup \{\hat{\mu}_1^{ua} \in I \not\equiv \hat{\mu}_2^{ua}\}\} \dots \\ &\quad \cup \{\{\hat{\mu}_2^{ua}, \hat{\mu}_1^{ua} \in I\} \cup \{\hat{\mu}_2^{ua} \in I \not\equiv \hat{\mu}_1\}\}\}^c \\ &= \{\{\overline{\Omega}_3 \cup \overline{\Omega}_2\} \cup \{\overline{\Omega}_3 \cup \emptyset\}\}^c = \{\overline{\Omega}_3 \cup \overline{\Omega}_2\}^c \\ &= \{\Omega_1\}. \end{aligned} \quad (46)$$

B. UCM displacing Newtonian

In the limit $R_\lambda^r \rightarrow 0$, we have $x^r, y^r, M^r \rightarrow 1$ and $z^r \rightarrow -3$. As a result, (31) reduces to

$$R_\eta^l \frac{\hat{\mu} z^l (\hat{\mu} + y^l)}{(\hat{\mu} + 1 - 2\hat{k}/3)(\hat{\mu} + x^l)} - 3\hat{\mu} R_\eta^r = \beta \hat{k}^3 - 2\hat{k} \llbracket R_\eta \rrbracket.$$

After some algebra, above can be written as ('un' stands for UCM and Newtonian) $\mathcal{F}^{un} = \sum_{j=0}^3 \hat{\mu}^j f_j^{un}(\hat{k}, \llbracket R_\eta \rrbracket, \beta) = 0$, where

$$\left. \begin{aligned} f_3^{un} &= 3(1 + \llbracket R_\eta \rrbracket)/2, \\ f_2^{un} &= s + f_3^{un}(M^l + x^l) + z^l(f_3^{un}/3 - 1), \\ f_1^{un} &= s(M^l + x^l) + f_3^{un}M^l x^l + y^l z^l(f_3^{un}/3 - 1), \\ f_0^{un} &= sM^l x^l, \quad s = \beta \hat{k}^3 - 2\hat{k} \llbracket R_\eta \rrbracket, \\ \beta &= \frac{1}{CaDe^2(3(U)/2)^3}, \quad M^l = 1 - 2\hat{k}/3. \end{aligned} \right\} \quad (47)$$

Denote by $\hat{\mu}_j^{un} = \hat{\mu}_j^{un}(\hat{k}, \llbracket R_\eta \rrbracket, \beta)$ for $j = 1, 2, 3$ the three roots of \mathcal{F}^{un} . Without loss of generality, we may assume $\Re\{\hat{\mu}_1^{un}\} \leq \Re\{\hat{\mu}_2^{un}\} \leq \Re\{\hat{\mu}_3^{un}\}$. The following (numerically obtained) are important to later development

$$z^l < -3, \quad 1 < x^l, y^l, \quad |M^l| < x^l, y^l. \quad (48)$$

B.1. Stable waveband

By definition, for $\llbracket R_\eta \rrbracket \in (-1, 1)$

$$f_3^{un}/3 - 1 < 0 < f_3^{un}. \quad (49)$$

In the long wave limit $\hat{k} \rightarrow 0$, we have $x^l, y^l \rightarrow 1$ and $z^l \rightarrow -3$, which in turn gives $\hat{\mu}_1^{un} \rightarrow -3f_3^{un}$, $\hat{\mu}_2^{un} \rightarrow -1$ and $\hat{\mu}_3^{un} \rightarrow 0$. Since $\hat{\mu}_1^{un}, \hat{\mu}_2^{un} < 0$ for sufficiently small \hat{k} by continuity, and $\prod_{j=1}^3 \hat{\mu}_j^{un} = -f_0^{un}/f_3^{un}$ by Vieta, it must be

(because $f_3^{un} > 0$) $\hat{\mu}_3^{un} < 0$ for small \hat{k} and only if $f_0^{un} > 0$ for small \hat{k} . By definition of f_0^{un} and (48), we conclude (i) if $\llbracket R_\eta \rrbracket \leq 0$, then $\hat{\mu}_3^{un} < 0$ for small \hat{k} , i.e. long waves are stable, and (ii) if $\llbracket R_\eta \rrbracket > 0$, then $\hat{\mu}_3^{un} > 0$ for small \hat{k} , i.e. long waves are unstable.

For \hat{k} bounded away from 0, the Routh-Hurwitz criterion states $\hat{\mu}_3^{un} < 0$ if and only if

$$f_0^{un} > 0, \quad f_2^{un} > 0, \quad f_2^{un} f_1^{un} - f_0^{un} f_3^{un} > 0. \quad (50)$$

By definitions and (48)

$$\left. \begin{aligned} \{f_0^{un} > 0\} &= \{\beta > \zeta_0 \mid \hat{k} < 3/2\} \cup \{\beta < \zeta_0 \mid \hat{k} > 3/2\}, \\ \{f_2^{un} > 0\} &= \{\beta > \zeta_2\}, \\ \{f_2^{un} f_1^{un} - f_0^{un} f_3^{un} > 0\} &= \{\mathcal{P} > 0\}, \end{aligned} \right\} \quad (51)$$

where

$$\left. \begin{aligned} \zeta_0 &= \frac{2\llbracket R_\eta \rrbracket}{\hat{k}^2}, \quad \zeta_2 = -\frac{f_3(M^l + x^l) + z^l(f_3/3 - 1)}{\hat{k}^3} + \zeta_0, \\ \mathcal{P} &= g_2 \hat{k}^6 \beta^2 + (g_1 - 2g_2 \hat{k}^3 \zeta_0) \hat{k}^3 \beta \dots \\ &\quad + (g_2 \hat{k}^6 \zeta_0^2 - g_1 \hat{k}^3 \zeta_0 + g_0), \\ g_2 &= M^l + x^l, \\ g_1 &= f_3(M^l + x^l)^2 \dots \\ &\quad + z^l(f_3/3 - 1)(M^l + x^l + y^l), \\ g_0 &= (f_3(M^l + x^l) + z^l(f_3/3 - 1)) \dots \\ &\quad \times (f_3 M^l x^l + y^l z^l(f_3/3 - 1)). \end{aligned} \right\} \quad (52)$$

First $\llbracket R_\eta \rrbracket \leq 0$. Since $\zeta_0 \leq 0$ by definition, the second part of the union of (51)₁ is empty (as $\beta > 0$), and the first part holds for all $\beta > 0$. In other words, $\hat{k} < 3/2$ is necessary for $\Re\{\hat{\mu}_3^{un}\} < 0$. To show this is also sufficient, we need to verify $\beta > \zeta_2$ and $\mathcal{P} > 0$ for $\hat{k} < 3/2$. Since $\zeta_0 \leq 0$ and by (49) and (48) we have $\zeta_2 < 0$, thus $\beta > \zeta_2$ for all $\beta > 0$. By (49) and (48), $g_1, g_2 > 0$. On the other hand, $\hat{k} < 3/2$ (so that $M^l > 0$) implies $g_0 > 0$. Since $\zeta_0 \leq 0$, we have $\mathcal{P} > 0$ for all $\beta > 0$. In summary

$$\{\Re\{\hat{\mu}_3^{un}\} < 0 \mid \llbracket R_\eta \rrbracket \leq 0\} = \{\hat{k} < 3/2\}.$$

Now consider $\llbracket R_\eta \rrbracket > 0$ (displaced fluid is more viscous). In this case, it is convenient to write (50) as the union of

$$\{\beta > \zeta_0 \mid \hat{k} < 3/2\} \cap \{\beta > \zeta_2\} \cap \{\mathcal{P} > 0\}, \quad (53)$$

and

$$\{\beta < \zeta_0 \mid \hat{k} > 3/2\} \cap \{\beta > \zeta_2\} \cap \{\mathcal{P} > 0\}. \quad (54)$$

First consider (53). Notice $\{\beta > \zeta_0 \mid \hat{k} < 3/2\} \subset \{\beta > \zeta_2\}$ because $\zeta_0 > \zeta_2$ by (49) and (48). Now we show $\{\beta >$

$\varsigma_0 \mid \hat{k} < 3/2\} \subset \{\mathcal{P} > 0\}$. Since \mathcal{P} is quadratic in β , its two roots can be easily obtained and given by

$$\left. \begin{aligned} \beta_1 &= \frac{-g_1 - (g_1^2 - 4g_0g_2)^{1/2}}{2g_2\hat{k}^3} + \varsigma_0, \\ \beta_2 &= \frac{-g_1 + (g_1^2 - 4g_0g_2)^{1/2}}{2g_2\hat{k}^3} + \varsigma_0. \end{aligned} \right\} \quad (55)$$

Since $g_2 > 0$ by (48), $\mathcal{P} > 0$ for all $\beta > 0$ if $g_1^2 - 4g_0g_2 < 0$. If $g_1^2 - 4g_0g_2 \geq 0$, then $\varsigma_0 \geq \beta_2$ for $\hat{k} < 3/2$ if and only if $(g_1^2 - 4g_0g_2)^{1/2} \leq g_1$, which is true because $g_2, g_1, g_0 \geq 0$ by (49) and (48), thus (53) is equivalent to

$$\{\beta > \varsigma_0 \mid \hat{k} < 3/2\}. \quad (56)$$

Now consider (54). It can be shown directly using the definitions that

$$g_1^2 - 4g_0g_2 = (f_3(M^l + x^l)^2 + z^l(f_3/3 - 1)(M^l + x^l - y^l))^2 \dots - 4(M^l + x^l)(f_3(M^l + x^l) + z^l(f_3/3 - 1))f_3M^lx^l.$$

Since $\hat{k} > 3/2$ (so that $M^l < 0$), we have $g_1^2 - 4g_0g_2 > 0$ by (49) and (48). As a result, (54) is equivalent to the union of

$$\{\beta < \varsigma_0 \mid \hat{k} > 3/2\} \cap \{\beta > \varsigma_2\} \cap \{\beta > \beta_2\}, \quad (57)$$

and

$$\{\beta < \varsigma_0 \mid \hat{k} > 3/2\} \cap \{\beta > \varsigma_2\} \cap \{\beta < \beta_1\}. \quad (58)$$

Notice $\mathcal{P}|_{\beta=\varsigma_2} = (f_3(M^l + x^l) + z^l(f_3/3 - 1))f_3M^lx^l$ is negative for $\hat{k} > 3/2$ by (49) and (48). This implies $\beta_1 \leq \varsigma_2 \leq \beta_2$ for $\hat{k} > 3/2$, which in turn implies (58) is empty and (57) is equivalent to $\{\beta_2 < \beta < \varsigma_0 \mid \hat{k} > 3/2\}$. As a result, (50) (provided $\llbracket R_\eta \rrbracket > 0$) is simply the union of the last set and (56). In summary

$$\begin{aligned} &\{\mathfrak{R}\{\hat{\mu}_3^{un}\} < 0 \mid \llbracket R_\eta \rrbracket > 0\} \\ &= \{\beta > \varsigma_0 \mid \hat{k} < 3/2\} \cup \{\beta_2 < \beta < \varsigma_0 \mid \hat{k} > 3/2\}. \end{aligned}$$

B.2. Stress singularity

Similar to the special case of UCM displacing air discussed in §5.1 and Appendix.A.2, the stress associated with $\hat{\mu}_j^{un}$ is singular if $\hat{\mu}_j^{un} \in I = [-M^l - \hat{k}, -M^l]$, which represents some volume regions in the $\hat{k}-\beta-\llbracket R_\eta \rrbracket$ space. For a few select $\llbracket R_\eta \rrbracket$ values, the cross-section of these singular regions are shown for $\hat{\mu}_1^{un}$, $\hat{\mu}_2^{un}$ and $\hat{\mu}_3^{un}$ in figure 13. Due to the complexity of the polynomial coefficients and the number of parameters involved, no exact expressions of the boundary curves are obtained. The main finding is as follows

- For sufficiently long waves (small \hat{k}), $\hat{\mu}_j^{un} \notin I$ for all $j = 1, 2, 3$ and $\llbracket R_\eta \rrbracket$ and β .
- For $\llbracket R_\eta \rrbracket \lesssim 1/2$, $\hat{\mu}_1^{un} \notin I$ for all β . For large $\llbracket R_\eta \rrbracket$ and small β , there can be multiple disjoint intervals of \hat{k} over which $\hat{\mu}_1^{un} \in I$ (see figure 13(a)). As β becomes larger, all such intervals shrink in size and eventually disappear (the threshold β value at which this happens decreases as $\llbracket R_\eta \rrbracket$ decreases).

- For large $\llbracket R_\eta \rrbracket$ and small β , there can be multiple disjoint intervals of \hat{k} over which $\hat{\mu}_2^{un} \in I$ (see figure 13(b)). Increasing β or decreasing $\llbracket R_\eta \rrbracket$ does not eliminate this and $\hat{\mu}_2^{un} \in I$ as \hat{k} becomes large enough.
- For all $\llbracket R_\eta \rrbracket$ and almost all β , $\hat{\mu}_3^{un} \in I$ as soon as \hat{k} becomes larger than $3/2$ (see figure 13(c)).

C. UCM displacing UCM

After some algebra, (31) can be rewritten as, $\mathcal{F} = \sum_{j=0}^4 \hat{\mu}^j f_j(\hat{k}, \llbracket R_\eta \rrbracket, \llbracket R_\lambda \rrbracket, \beta) = 0$ where

$$\left. \begin{aligned} f_4 &= (R_\lambda^l R_\eta^r z^r + R_\lambda^r R_\eta^l z^l) R_\lambda^l R_\lambda^r - s(R_\lambda^r R_\lambda^l)^2, \\ f_3 &= (R_\lambda^r \hat{x}^l + R_\lambda^l y^r) R_\lambda^l R_\eta^r z^r \dots \\ &\quad + (R_\lambda^l \hat{x}^r + R_\lambda^r y^l) R_\lambda^r R_\eta^l z^l - s R_\lambda^r R_\lambda^l (R_\lambda^r \hat{x}^l + R_\lambda^l \hat{x}^r), \\ f_2 &= (R_\lambda^l \hat{x}^l y^r + R_\lambda^r \hat{x}^l) R_\eta^r z^r \dots \\ &\quad + (R_\lambda^r \hat{x}^r y^l + R_\lambda^l \hat{x}^r) R_\eta^l z^l - s(R_\lambda^r R_\lambda^l \hat{x}^l \hat{x}^r + R_\lambda^{l,2} \hat{x}^l + R_\lambda^{r,2} \hat{x}^r), \\ f_1 &= \hat{x}^l y^r R_\eta^r z^r + \hat{x}^r y^l R_\eta^l z^l - s(R_\lambda^l \hat{x}^l \hat{x}^r + R_\lambda^r \hat{x}^r \hat{x}^l), \\ f_0 &= -s \hat{x}^l \hat{x}^r, \\ \hat{x}^l &= M^l x^l, \quad \hat{x}^r = M^r x^r, \\ \hat{x}^l &= M^l + x^l, \quad \hat{x}^r = M^r + x^r. \\ M^l &= 1 - 2R_\lambda^l \hat{k}/3, \quad M^r = 1 + 2R_\lambda^r \hat{k}/3, \\ \beta &= 1/(CaDe^2(3\langle U \rangle/2)^3), \quad s = \beta \hat{k}^3 - 2\hat{k} \llbracket R_\eta \rrbracket \end{aligned} \right\} \quad (59)$$

Denote by $\{\hat{\mu}_j\}_{j=1}^4$ the four roots of \mathcal{F} . Without loss of generality, we may assume $\mathfrak{R}\{\hat{\mu}_1\} \leq \mathfrak{R}\{\hat{\mu}_2\} \leq \mathfrak{R}\{\hat{\mu}_3\} \leq \mathfrak{R}\{\hat{\mu}_4\}$. Numerical results show

$$\left. \begin{aligned} z^l < 0, \quad 1 < x^l, y^l, \quad z^r < 0 < x^r. \\ x^r, x^l, y^r, y^l \rightarrow 1, \quad z^r, z^l \rightarrow -3, \quad \text{as } \hat{k} \rightarrow 0. \end{aligned} \right\} \quad (60)$$

C.1. Long wave stability

Viscous effect is still the dominant mechanism in determining stability for long waves. If the displacing fluid is more or equally viscous than the displaced fluid ($\llbracket R_\eta \rrbracket \leq 0$), the flow is stable to sufficiently long wave, and unstable if the displaced fluid is more viscous ($\llbracket R_\eta \rrbracket > 0$). This can be seen by examining the sign of $\mathfrak{R}\{\hat{\mu}_4\}$ for sufficiently small \hat{k} .

Let f_j^* s be the limits of f_j s as $\hat{k} \rightarrow 0$. By definitions (59) and (60), it is straightforward to show that $f_4^* = -3(R_\lambda^l R_\eta^r + R_\lambda^r R_\eta^l) R_\lambda^l R_\lambda^r$, $f_3^* = -3(R_\lambda^l R_\eta^r + R_\lambda^r R_\eta^l + R_\lambda^l R_\lambda^r)$,

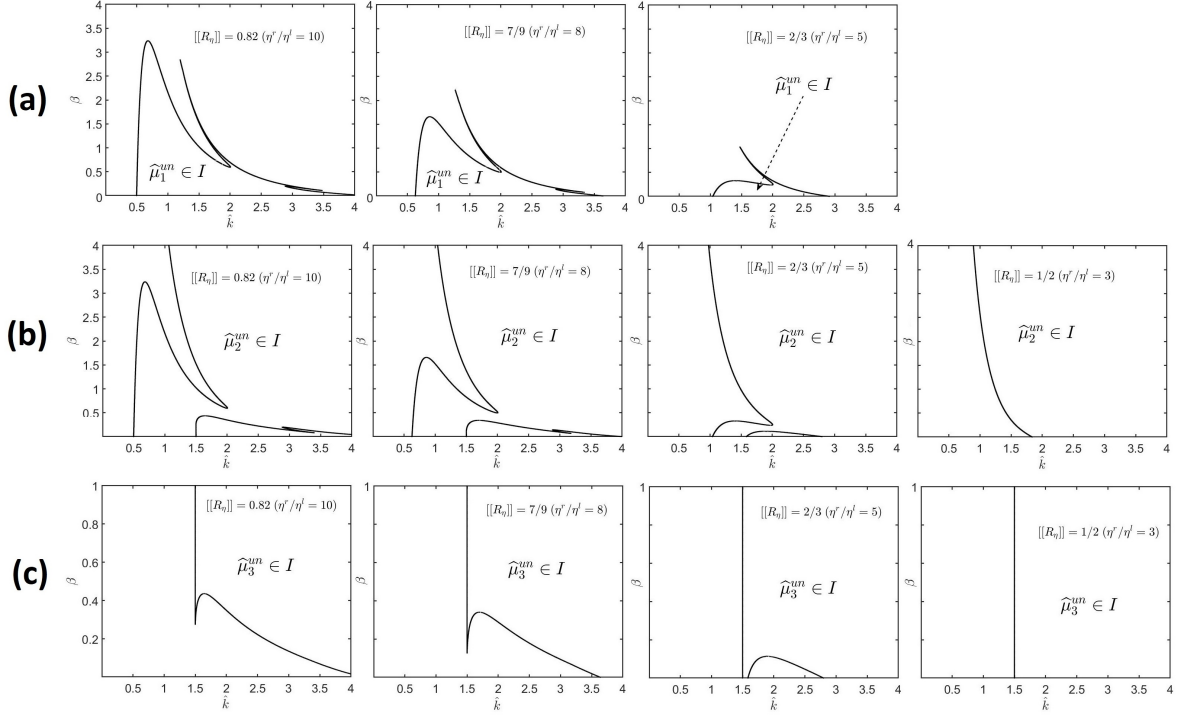


Figure 13: The region where $\hat{\mu}_i^{un} \in I$ is shown in $\hat{k} - \beta$ plane with select $\llbracket R_\eta \rrbracket$ values.

$f_2^* = -3(R_\lambda^l R_\eta^r + R_\lambda^r R_\eta^l + 1)$, $f_1^* = -3$ and $f_0^* = 0$. As a result, $\mathcal{F} \xrightarrow{\hat{k} \rightarrow 0} \mathcal{F}^*$, where $\mathcal{F}^* = \hat{\mu}(f_4^* \hat{\mu}^3 + f_3^* \hat{\mu}^2 + f_2^* \hat{\mu} + f_1^*)$. Evidently, $\{\hat{\mu}_j\}_{j=1}^4$ must converge to the four roots of \mathcal{F}^* , denoted by $\{\hat{\mu}_j^*\}_{j=1}^4$. It can be shown $\{\hat{\mu}_j^*\}_{j=1}^3 = \{-1/R_\lambda^l, -1/(R_\lambda^l R_\eta^r + R_\lambda^r R_\eta^l), -1/R_\lambda^r\}$ and $\hat{\mu}_4^* = 0$. Since the limits of $\hat{\mu}_j$ for $j = 1, 2, 3$ are negative as $\hat{k} \rightarrow 0$, they remain negative for small \hat{k} by continuity. Since $\prod_{j=1}^3 \hat{\mu}_j < 0$ for small \hat{k} and $\prod_{j=1}^4 \hat{\mu}_j = f_0/f_4$, the sign of $\hat{\mu}_4$ is the same as $-f_0/f_4$ for small \hat{k} . Since $f_4 < 0$ for small \hat{k} , the sign of $\hat{\mu}_4$ is the same as $f_0 := -s\check{x}^l\check{x}^r$ for small \hat{k} , which is the same as that of $-s$ because $\check{x}^l\check{x}^r \xrightarrow{\hat{k} \rightarrow 0} 1$. By definition of s , we conclude $\hat{\mu}_4 < 0$ for small \hat{k} if and only if $\llbracket R_\eta \rrbracket \leq 0$.

For \hat{k} bounded away from 0, we will consider $\llbracket R_\eta \rrbracket \leq 0$ and $\llbracket R_\eta \rrbracket > 0$ separately in §C.2 and §C.3.

C.2. Displacing fluid is more viscous: $\llbracket R_\eta \rrbracket \leq 0$

By Routh-Hurwitz criterion, $\Re\{\hat{\mu}_4\} < 0$ if and only if

$$\left. \begin{aligned} f_3/f_4 > 0, \quad f_1/f_4 > 0, \\ f_0/f_4 > 0, \quad (f_3 f_2 f_1 - f_1^2 f_4 - f_3^2 f_0)/f_4^3 > 0. \end{aligned} \right\} \quad (61)$$

Since $s > 0$ for $\llbracket R_\eta \rrbracket \leq 0$ and $z^l, z^r < 0$, it follows from definition that $f_4 < 0$, thus (61) becomes

$$f_3, f_1, f_0, f_3 f_2 f_1 - f_1^2 f_4 + f_3^2 f_0 < 0. \quad (62)$$

Since $\check{x}^r := M^r x^r > 0$, and $s > 0$, we have $f_0 < 0 \Leftrightarrow \check{x}^l > 0$. In other words, $\Re\{\hat{\mu}_4\} \geq 0$ if $\check{x}^l \leq 0$. Since $x^l > 0$, $\check{x}^l := M^l x^l \leq 0 \Leftrightarrow M^l := 1 - 2R_\lambda^l \hat{k}/3 \leq 0$. As a result, $\Re\{\hat{\mu}_4\} \geq 0$ if $\hat{k} \geq 3/(2R_\lambda^l)$. For $\hat{k} < 3/(2R_\lambda^l)$, numerical result shows (62) holds (so that $\Re\{\hat{\mu}_4\} < 0$) for all β and $\llbracket R_\lambda \rrbracket$ (provided $\llbracket R_\eta \rrbracket \leq 0$), thus the marginal curve is simply given by $\hat{k} = 3/(2R_\lambda^l)$.

C.3. Displaced fluid is more viscous: $\llbracket R_\eta \rrbracket > 0$

C.3.1. Resonance

In Appendix.C.1, it has been established that $f_4 < 0$ for small \hat{k} regardless the values of $\llbracket R_\eta \rrbracket$, $\llbracket R_\lambda \rrbracket$ and β . If, as \hat{k} increases, f_4 vanishes at some $\hat{k} = \hat{k}_*(\llbracket R_\eta \rrbracket, \llbracket R_\lambda \rrbracket, \beta)$ (there can be multiple solutions to $f_4 = 0$ in general but we consider only the smallest \hat{k}_* value), then at least one of $\{\hat{\mu}_j\}_{j=1}^4$ must become unbounded as $\hat{k} \rightarrow \hat{k}_*$ (because they are polynomial roots). Numerical result shows $f_3|_{\hat{k}=\hat{k}_*} > 0$ (see Remark below for a justification), thus \mathcal{F} can at most degenerate to a cubic polynomial rather than quadratic at $\hat{k} = \hat{k}_*$. This implies only one of $\hat{\mu}_j$ s will diverge as $\hat{k} \rightarrow \hat{k}_*$, and must diverge along the real line (otherwise there must be two roots diverging to infinity as complex conjugates but \mathcal{F} cannot degenerate to quadratic). To determine whether it diverges to $-\infty$ or $+\infty$, we notice $f_4 < 0$ for $\hat{k} \in (0, \hat{k}_*)$ and $f_3 > 0$ at $\hat{k} = \hat{k}_*$, thus $f_3/f_4 < 0$ over $\hat{k} \in (\hat{k}_* - \epsilon, \hat{k}_*)$ for sufficiently small ϵ . Since only one of the roots diverges, it must diverge to $+\infty$ as $\hat{k} \rightarrow \hat{k}_*$ because $\sum_{j=1}^4 \hat{\mu}_j = -f_3/f_4$ by Vieta (the sum is positive and dominated by the diverging root near \hat{k}_*).

By definition, $f_4 \leq 0$ if and only if $\beta \geq \zeta$, where

$$\zeta \stackrel{def}{=} (R_\eta^r z^r / R_\lambda^r + R_\eta^l z^l / R_\lambda^l + 2\hat{k} \llbracket R_\eta \rrbracket) / \hat{k}^3 \quad (63)$$

As a result, $f_4 < 0$ for all \hat{k} if and only if $\beta > \beta_*(\llbracket R_\eta \rrbracket, \llbracket R_\lambda \rrbracket)$, where $\beta_* \stackrel{def}{=} \max_{\hat{k}} \zeta(\hat{k}, \llbracket R_\eta \rrbracket, \llbracket R_\lambda \rrbracket)$. In other words, $\hat{\mu}_4 \rightarrow +\infty$ as $\hat{k} \rightarrow \hat{k}_*$ if $\beta \leq \beta_*$.

Remark: It can be shown $f_3|_{\hat{k}=\hat{k}_*} = R_\lambda^{l,2} R_\eta^r (y^r - \hat{x}^r) z^r + R_\lambda^{r,2} R_\eta^l (y^l - \hat{x}^l) z^l|_{\hat{k}=\hat{k}_*}$. The first term is always positive, thus $f_3|_{\hat{k}=\hat{k}_*} > 0$ if and only if

$$R_\eta^r / R_\lambda^r > -(R_\lambda^r / R_\lambda^l)^2 \frac{(y^l - \hat{x}^l) z^l}{(y^r - \hat{x}^r) z^r} \Big|_{\hat{k}=\hat{k}_*}.$$

The right hand side of the above inequality is a function of \hat{k} and $\llbracket R_\lambda \rrbracket$ whose maximum is approximately 2.333, thus the inequality holds if $R_\eta^r / R_\lambda^r \gtrsim 2.333$ (equivalently $\llbracket R_\eta \rrbracket \gtrsim 0.4$). Since $f_4 = 0$ can only occur for $\llbracket R_\eta \rrbracket \gtrsim 0.797$, thus the inequality holds so that $f_3 > 0$ whenever $f_4 = 0$.

C.3.2. Stable waveband

For $\beta \gtrsim 1.113$, $f_4 < 0$ always, thus Routh-Hurwitz criterion (61) states $\Re\{\hat{\mu}_4\} < 0$ iff $f_3, f_1, f_0, f_3 f_2 f_1 - f_1^2 f_4 - f_3^2 f_0 < 0$. Since $M^r, x^l, x^r > 0$, then by definition $f_0 < 0$ iff $\hat{k} \in (\min\{\hat{k}_o, \hat{k}_*\}, \max\{\hat{k}_o, \hat{k}_*\})$, where $\hat{k}_* = 3/(2R_\lambda^l)$ and $\hat{k}_o = (2\llbracket R_\eta \rrbracket / \beta)^{1/2}$. By definition, $\hat{k}_o < \hat{k}_*$ iff $8R_\lambda^{l,2} \llbracket R_\eta \rrbracket / 9 < \beta$ and the left hand side of the last inequality is at most $8/9$, thus it holds for $\beta \gtrsim 1.113$. In other words, the stable wave range ($\Re\{\hat{\mu}_4\} < 0$) must be contained in the interval (\hat{k}_o, \hat{k}_*) because $f_0 \geq 0$ otherwise. In fact, numerical results show the whole interval contains only stable waves, thus the marginal curves are given by $\hat{k} = \hat{k}_o$ and $\hat{k} = \hat{k}_*$.

C.4. Stress singularity

It is clear from the beginning part of §5 that $\tilde{\tau}^{xx,l}$ and $\tilde{\tau}^{xx,r}$ are assumed a priori to be integrable across the cell gap $y \in (-1, 1)$, which requires ψ^l and ψ^r given by (23)₄ and (24)₄ to be non-zero over $y \in [-1, 1]$. In particular, $\psi^l \neq 0$ for $y \in [-1, 1]$ iff

$$\left. \begin{aligned} &\hat{\mu} \notin [W_1^l, W_2^l], \\ &W_1^l = -\hat{k}/3 - 1/R_\lambda^l, \quad W_2^l = 2\hat{k}/3 - 1/R_\lambda^l. \end{aligned} \right\} \quad (64)$$

Similarly, $\psi^r \neq 0$ for $y \in [-1, 1]$ iff

$$\left. \begin{aligned} &\hat{\mu} \notin [W_1^r, W_2^r], \\ &W_1^r = -2\hat{k}/3 - 1/R_\lambda^r, \quad W_2^r = \hat{k}/3 - 1/R_\lambda^r. \end{aligned} \right\} \quad (65)$$

As a result, $\psi^l, \psi^r \neq 0$ over $y \in [-1, 1]$ iff

$$\hat{\mu} \notin W, \quad W = [W_1^l, W_2^l] \cup [W_1^r, W_2^r]. \quad (66)$$

In other words, if $\hat{\mu} = \hat{\mu}_j$ does not satisfy (66), then the stress associated with $\hat{\mu}_j$ is singular. To see this is an effect of elasticity, we may express (64) in dimensional forms (superscript $*$) $\mu^* \notin [-|k^*| \langle U^* \rangle / 2 - 1/\lambda^l, |k^*| \langle U^* \rangle - 1/\lambda^l]$, which is satisfied for any finite μ^* if $\lambda^l \rightarrow 0$. Similarly, dimensional form of (65) is given by $\mu^* \notin [-|k^*| \langle U^* \rangle - 1/\lambda^r, |k^*| \langle U^* \rangle / 2 - 1/\lambda^r]$, which is satisfied if $\lambda^r \rightarrow 0$.

Now we show the singular regions for $j = 1, 2, 3, 4$ using the rheological data from the experiments of [32], where the authors used six UCM-like fluids with different viscosities η and relaxation times λ . A linear fit among the provided data gives $\hat{\lambda} = 0.2435\hat{\eta} + 1.4678$, where $\hat{\eta}$ and $\hat{\lambda}$ are the values of η and λ measured in Ns/m^2 and $10^{-1}s$. According to this linear relation, we compute $\hat{\lambda}$ for fixed $\hat{\eta}$ at 1, 5 and 10 to obtain

$$(\hat{\eta}, \hat{\lambda}) = (1, 1.7113), \quad (5, 2.6853), \quad (10, 3.9028). \quad (67)$$

If $(\hat{\eta}^l, \hat{\lambda}^l) = (67)_1$ and $(\hat{\eta}^r, \hat{\lambda}^r) = (67)_2$, then the associated $\llbracket R_\eta \rrbracket$ and $\llbracket R_\lambda \rrbracket$ can be computed. By choosing all possible combinations from (67), we obtain

$$\llbracket R_\eta \rrbracket, \llbracket R_\lambda \rrbracket = \begin{cases} (-1/3, 0.185), & (-2/3, 0.2215), \\ (-0.82, 0.39), & (1/3, 0.185), \\ (2/3, 0.2215), & (0.82, 0.39). \end{cases} \quad (68)$$

1. For $(\llbracket R_\eta \rrbracket, \llbracket R_\lambda \rrbracket)$ given by (68)₁, (68)₂ or (68)₃, we find for $\beta \in (0, 100)$

- $\hat{\mu}_1, \hat{\mu}_2, \hat{\mu}_3 \notin W$ for all \hat{k}
- $\hat{\mu}_4 \notin W$ only upto $\hat{k} = \hat{k}_* := 3/(1 - \llbracket R_\lambda \rrbracket)$.

2. For $(\llbracket R_\eta \rrbracket, \llbracket R_\lambda \rrbracket)$ given by (68)₄, we find

- $\hat{\mu}_1 \notin W$ for $\beta \in (0, 100)$.
- $\hat{\mu}_2, \hat{\mu}_3 \notin W$ if $\beta \lesssim 23$. For larger β values, $\hat{\mu}_2, \hat{\mu}_3 \notin W$ only for \hat{k} up to some β dependent value. See figure 14a.
- for $\beta \lesssim 87$, $\hat{\mu}_4 \notin W$ up to $\hat{k} = \hat{k}_* := 3/(1 - \llbracket R_\lambda \rrbracket) \approx 3.68$. For larger β values, there is another branch over which $\hat{\mu}_4 \in W$. See figure 14b.

3. For $(\llbracket R_\eta \rrbracket, \llbracket R_\lambda \rrbracket)$ given by (68)₅, we find

- $\hat{\mu}_1 \notin W$ for $\beta \in (0, 100)$.
- $\hat{\mu}_2, \hat{\mu}_3 \notin W$ if $\beta \lesssim 10.4$. For larger β values, $\hat{\mu}_2, \hat{\mu}_3 \notin W$ only for \hat{k} up to some β dependent value. See figure 15a.
- for $\beta \lesssim 10.4$, $\hat{\mu}_4 \in W$ up to $\hat{k} = \hat{k}_* := 3/(1 - \llbracket R_\lambda \rrbracket) \approx 3.85$. For larger β values, there is another branch over which $\hat{\mu}_4 \in W$. See figure 15b.

4. For $(\llbracket R_\eta \rrbracket, \llbracket R_\lambda \rrbracket)$ given by (68)₆, we find

- $\hat{\mu}_1 \notin W$ if $\beta \lesssim 9.3$. For larger β values, $\hat{\mu}_1 \notin W$ only for \hat{k} up to some β dependent value. See figure 16a.

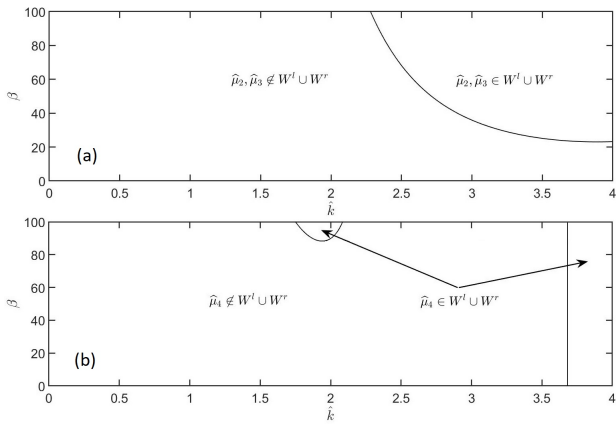


Figure 14: For $(\llbracket R_\eta \rrbracket, \llbracket R_\lambda \rrbracket) = (1/3, 0.185)$, the regions where $\hat{\mu}_j \in W$ are shown.

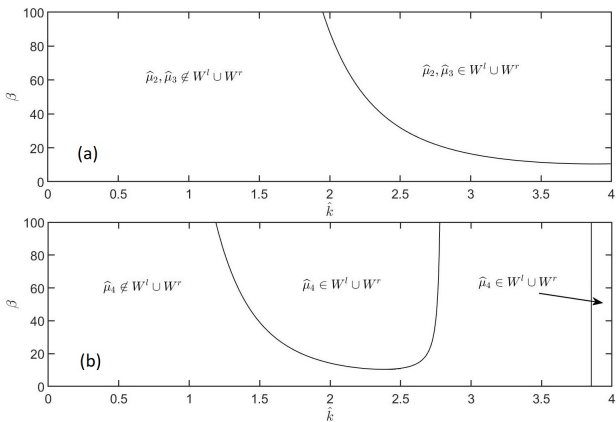


Figure 15: For $(\llbracket R_\eta \rrbracket, \llbracket R_\lambda \rrbracket) = (2/3, 0.2215)$, the region where $\hat{\mu}_j \in W$ is shown.

- $\hat{\mu}_2, \hat{\mu}_3 \notin W$ if $\beta \lesssim 4.5$. For larger β values, $\hat{\mu}_2, \hat{\mu}_3 \in W$ only for \hat{k} up to some β dependent value. See figure 16b.
- $\hat{\mu}_4 \notin W$ for \hat{k} up to some β dependent value. See figure 16c.

References

- [1] AHMADIKHAMSI, S., GOLFIER, F., OLTEAN, C., LEFÈVRE, ERIC & BAHRANI, S AMIR 2020 Impact of surfactant addition on non-newtonian fluid behavior during viscous fingering in hele-shaw cell. *Physics of Fluids* **32** (1), 012103. doi: 10.1063/1.5128589.
- [2] BALL, T., BALMFORTH, N. & DUFRESNE, A. 2021 Viscoplastic fingers and fractures in a Hele-Shaw cell. *Journal of Non-Newtonian Fluid Mechanics* **289**, 104492. doi: 10.1016/j.jnnfm.2021.104492
- [3] BEN AMAR, M. & POIRE, E. 1999 Pushing a non-Newtonian fluid in a Hele-Shaw cell: From fingers to needles. *Physics of Fluids* **11**, 1757–1767. doi: 10.1063/1.870041
- [4] BIRD, R. B., CURTISS, C. F., ARMSTRONG, R. C. & HASSAGER, O. 1987 *Dynamics of Polymeric Liquids, Volume 2: Kinetic Theory*. Wiley.
- [5] BONN, D., KELLAY, H., BEN AMAR, M. & MEUNIER, J. 1995 Viscous finger widening with surfactants and polymers. *Physical review letters* **75**, 2132–2135. doi: 10.1103/PhysRevLett.75.2132.

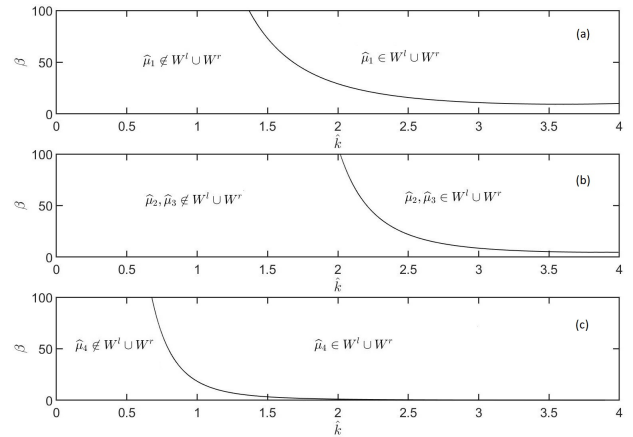


Figure 16: For $(\llbracket R_\eta \rrbracket, \llbracket R_\lambda \rrbracket) = (0.82, 0.39)$, the region where $\hat{\mu}_j \in W$ is shown.

- [6] BUKA, A., KERTESZ, J. & VICSEK, T. 1986 Transitions of viscous fingering patterns in nematic liquid crystals. *Nature* **323**, 424–425. doi: 10.1038/323424a0.
- [7] CASADEMUNT, J. 2004 Viscous fingering as a paradigm of interfacial pattern formation: Recent results and new challenges. *Chaos: An Interdisciplinary Journal of Nonlinear Science* **14** (3), 809–824. doi: 10.1063/1.1784931.
- [8] CHEN, K. 1991 Interfacial instability due to elastic stratification in concentric coextrusion of two viscoelastic fluids. *Journal of non-newtonian fluid mechanics* **40** (2), 155–175. doi: 10.1016/0377-0257(91)85011-7.
- [9] COUSSOT, P. 1999 Saffman–Taylor instability in yield-stress fluids. *Journal of Fluid Mechanics* **380**, 363 – 376. doi: 10.1017/S002211209800370X.
- [10] DACCORD, G., NITTMANN, J. & STANLEY, H. 1986 Radial viscous fingers and diffusion-limited aggregation: Fractal dimension and growth sites. *Physical review letters* **56**, 336–339. doi: 10.1103/PhysRevLett.56.336.
- [11] DARIPA, P. 2013 Saffman-Taylor instability for a non-Newtonian fluid. *Bull. Amer. Phys. Soc.* **58** (18), 421.
- [12] DARIPA, P. 2014 Instability of displacement of an Oldroyd-B fluid by air in a Hele-Shaw cell. *Bull. Amer. Phys. Soc.* **59** (1).
- [13] DRAZIN, P. & REID, W. 2004 *Hydrodynamic Stability*. Cambridge University Press. doi: 10.1017/CBO9780511616938.
- [14] ESLAMI, A. & TAGHAVI, S.M. 2017 Viscous fingering regimes in elasto-visco-plastic fluids. *Journal of Non-Newtonian Fluid Mechanics* **243**, 79–94. doi: 10.1016/j.jnnfm.2017.03.007.
- [15] ESLAMI, A & TAGHAVI, SM 2020 Viscoplastic fingering in rectangular channels. *Physical Review E* **102** (2), 023105. doi: 10.1103/PhysRevE.102.023105.
- [16] FAST, P., KONDIC, L., SHELLEY, M. & PALFFY-MUHORAY, P. 2001 Pattern formation in non-Newtonian Hele-Shaw flow. *Physics of Fluids* **13**, 1191–1212. doi: 10.1063/1.1359417.
- [17] FONTANA, J., DIAS, E. & MIRANDA, J. 2014 Controlling and minimizing fingering instabilities in non-Newtonian fluids. *Physical review E* **89**. doi: 10.1103/PhysRevE.89.013016.
- [18] GHOSH, S., MANDAL, T.K., DAS, G. & DAS, P.K. 2009 Review of oil water core annular flow. *Renewable and Sustainable Energy Reviews* **13** (8), 1957–1965. doi: 10.1016/j.rser.2008.09.034.
- [19] GOVINDARAJAN, R. & SAHU, K.C. 2014 Instabilities in viscosity-stratified flow. *Annu. Rev. Fluid Mech* **46** (1), 331–353. doi: 10.1146/annurev-fluid-010313-141351.
- [20] HAI, Z. & DARIPA, P. 2022 Linear instability of viscoelastic interfacial Hele-Shaw flows: Newtonian fluid displacing UCM fluid. *Journal of Non-Newtonian Fluid Mechanics* **303**, 104773. doi: 10.1016/j.jnnfm.2022.104773.
- [21] HILL, S. 1952 Channeling in packed columns. *Chem. Eng. Sci.* **1**,

- 247–253. doi: 10.1016/0009-2509(52)87017-4.
- [22] HOMSY, G. 1987 Viscous fingering in porous media. *Annual Review of Fluid Mechanics* **19**, 271–311. doi: 10.1146/annurev.fl.19.010187.001415.
- [23] KONDIC, L., PALFFY-MUHORAY, P. & SHELLEY, M. 1996 Models of Non-Newtonian Hele-Shaw flow. *Physical review E* **54**, R4536–R4539. doi: 10.1103/PhysRevE.54.R4536.
- [24] KONDIC, L., SHELLEY, M. & PALFFY-MUHORAY, P. 1998 Non-Newtonian Hele-Shaw flow and the Saffman-Taylor instability. *Physical Review Letters* **80**. doi: 10.1103/PhysRevLett.80.1433.
- [25] LEMAIRE, E., LEVITZ, P., DACCORD, G. & VAN DAMME, H. 1991 From viscous fingering to viscoelastic fracturing in colloidal fluids. *Physical review letters* **67**, 2009–2012. doi: 10.1103/PhysRevLett.67.2009.
- [26] LINDNER, A., BONN, D. & MEUNIER, J. 2000 Viscous fingering in a shear-thinning fluid. *Physics of Fluids* **12**, 256–261. doi: 10.1063/1.870303.
- [27] LINDNER, A., BONN, D., POIRE, E., BEN AMAR, M. & J., MEUNIER 2002 Viscous fingering in non-Newtonian fluids. *Journal of Fluid Mechanics* **469**, 237 – 256. doi: 10.1017/S0022112002001714.
- [28] LINDNER, A., COUSSOT, P. & D., BONN 2000 Viscous fingering in a yield stress fluid. *Physical review letters* **85**, 314–7. doi: 10.1103/PhysRevLett.85.314.
- [29] MALEKI-JIRSARAEI, N., LINDNER, A., ROUHANI, S. & BONN, D. 2005 Saffman-Taylor instability in yield stress fluids. *Journal of Physics: Condensed Matter* **17** (14), S1219–S2228. doi: 10.1088/0953-8984/17/14/011.
- [30] MCCLOUD, K. & MAHER, J. 1995 Experimental perturbations to Saffman-Taylor flow. *Physics Reports* **260**, 139–185. doi: 10.1016/0370-1573(95)91133-U.
- [31] MORA, S. & MANNA, M. 2009 Saffman-Taylor instability for generalized Newtonian fluids. *Physical review E* **80**, 016308. doi: 10.1103/PhysRevE.80.016308.
- [32] MORA, S. & MANNA, M. 2012 From viscous fingering to elastic instabilities. *Journal of Non-Newtonian Fluid Mechanics* **173–174**, 30–39. doi: 10.1016/j.jnnfm.2012.01.010.
- [33] MOROZOV, A. & SPAGNOLIE, S. 2015 Introduction to complex fluids. In *Spagnolie, S. (eds) Complex Fluids in Biological Systems*, pp. 3–52. New York, NY: Springer. doi: 10.1007/978-1-4939-2065-5_1.
- [34] NASE, J., LINDNER, A. & CRETON, C. 2008 Pattern formation during deformation of a confined viscoelastic layer: From a viscous liquid to a soft elastic solid. *Physical review letters* **101**, 074503. doi: 10.1103/PhysRevLett.101.074503.
- [35] NITTMANN, J., DACCORD, G. & STANLEY, H. 1985 Fractal growth of viscous fingers: quantitative characterization of a fluid instability phenomenon. *Nature* **314**, 141–144. doi: 10.1038/314141a0.
- [36] PARK, C. & HOMSY, G. 1984 Two-phase displacement in Hele-Shaw cells: Theory. *Journal of Fluid Mechanics* **139**, 291 – 308. doi: 10.1017/S0022112084000367.
- [37] PARK, S. & DURIAN, D. 1994 Viscous and elastic fingering instabilities in foam. *Physical review letters* **72**, 3347–3350. doi: 10.1103/PhysRevLett.72.3347.
- [38] REINELT, D. A. 1987 Interface conditions for two-phase displacement in Hele-Shaw cells. *Journal of Fluid Mechanics* **183**, 219–234. doi: 10.1017/S0022112087002611.
- [39] RENARDY, M. 2000 *Mathematical Analysis of Viscoelastic Flows*. SIAM. doi: 10.1137/1.9780898719413
- [40] RENARDY, Y. 1985 Instability at the interface between two shearing fluids in a channel. *The Physics of fluids* **28** (12), 3441–3443. doi: 10.1063/1.865346.
- [41] RO, J. S. & HOMSY, G. M. 1995 Viscoelastic free surface flows: thin film hydrodynamics of Hele-Shaw and dip coating flows. *Journal of Non-Newtonian Fluid Mechanics* **57** (2-3), 203–225. doi: 10.1016/0377-0257(94)01329-G.
- [42] SADER, J., CHAN, D. & HUGHES, B. 1994 Non-Newtonian effects on immiscible viscous fingering in a radial Hele-Shaw cell. *Physical review E* **49**, 420–432. doi: 10.1103/PhysRevE.49.420
- [43] SAFFMAN, P. 1986 Viscous fingering in Hele-Shaw cells. *Journal of Fluid Mechanics* **173**. doi: 10.1017/S0022112086001088.
- [44] SAFFMAN, P. G. & TAYLOR, G. 1958 Penetration of a fluid into a porous medium or Hele-Shaw cell containing a more viscous liquid. *Proceedings of The Royal Society A: Mathematical, Physical and Engineering Sciences* **245**, 312–329. doi: 10.1098/rspa.1958.0085.
- [45] SAINTYVES, B., DAUCHOT, O. & BOUCHAUD, E. 2012 Bulk elastic fingering instability in Hele-Shaw cells. *Physical review letters* **111**. doi: 10.1103/PhysRevLett.111.047801.
- [46] SAINTYVES, B., MORA, S. & BOUCHAUD, E. 2019 A meniscus fingering instability in viscoelastic fluids. *Physics of Fluids* **31** (6), 063108. doi: 10.1063/1.5097685.
- [47] SHOKRI, H., KAYHANI, M.H. & NOROUZI, M. 2018 Saffman-taylor instability of viscoelastic fluids in anisotropic porous media. *International Journal of Mechanical Sciences* **135**, 1–13. doi: 10.1016/j.ijmecsci.2017.11.008.
- [48] VAN DAMME, H., ALSAC, E., LAROCHE, C. & GATINEAU, L. 1988 On the respective roles of low surface tension and non-Newtonian rheological properties in fractal fingering. *Europhysics Letters (EPL)* **5**, 573–573. doi: 10.1209/0295-5075/5/6/016.
- [49] VAN DAMME, H., LEMAIRE, E., OULD, Y., ABDELHAYE, M., MOURCHID, A. & LEVITZ, P. 1994 Pattern formation in particulate complex fluids: A guided tour. In *Non-linearity and breakdown in soft condensed matter*, pp. 134–150. Springer. doi: 10.1007/3-540-58652-0_34.
- [50] VAN DAMME, H., OBRECHT, F., LEVITZ, P., GATINEAU, L. & LAROCHE, C. 1986 Fractal viscous fingering in clay slurries. *Nature* **320** (6064), 731–733. doi: 10.1038/320731a0.
- [51] WILSON, S.D.R 1990 The Taylor-Saffman problem for a non-Newtonian liquid. *Journal of Fluid Mechanics* **220**, 413 – 425. doi: 10.1017/S0022112090003329.
- [52] YIH, CHIA-SHUN 1967 Instability due to viscosity stratification. *Journal of Fluid Mechanics* **27** (2), 337–352. doi: 10.1017/S0022112067000357.
- [53] ZHAO, H. & MAHER, J. V. 1993 Associating-polymer effects in a Hele-Shaw experiment. *Phys. Rev. E.* **47**, 4278 – 4283. doi: 10.1103/PhysRevE.47.4278.